High-resolution respirometry reveals altered mammalian tissue ketone body oxidation in different cardiometabolic diseases

Elric Zweck[1,2,3,4,10], Sarah Piel[3,4,10], Johannes W. Schmidt[3,4], Daniel Scheiber[1,2,3,4], Martin Schön[1,2,5], Sabine Kahl[1,2,5], Volker Burkart[1,2], Bedair Dewidar[1,2], Ricarda Remus[3,4], Alexandra Chadt[2,6], Hadi Al-Hasani[2,6], Hug Aubin[4,7], Udo Boeken[7], Artur Lichtenberg[4,7], Amin Polzin[3,4], Malte Kelm[3,4], Ralf Westenfeld[3,4], Robert Wagner[1,2,5], Julia Szendroedi[1,2,8,9], Michael Roden[1,2,5,11], Cesare Granata[1,2,11,12*]

[1]Institute for Clinical Diabetology, German Diabetes Center, Leibniz Center for Diabetes Research, Heinrich-Heine-University Düsseldorf, Düsseldorf, Germany

[2]German Center for Diabetes Research (DZD e.V.), Partner Düsseldorf, Munich-Neuherberg, Germany

[3]Department of Cardiology, Pulmonology, and Vascular Medicine, Medical Faculty, Heinrich-Heine-University Düsseldorf, Düsseldorf, Germany

[4]CARID, Cardiovascular Research Institute Düsseldorf, Medical Faculty, Heinrich-Heine-University Düsseldorf, Düsseldorf, Germany

[5]Department of Endocrinology and Diabetology, Medical Faculty, Heinrich-Heine-University Düsseldorf, Düsseldorf, Germany

[6]Institute for Clinical Biochemistry and Pathobiochemistry, German Diabetes Center, Leibniz Center for Diabetes Research at Heinrich-Heine-University Düsseldorf, Düsseldorf, Germany

[7]Department of Cardiac Surgery, Medical Faculty, Heinrich-Heine-University Düsseldorf, Düsseldorf, Germany

[8]Department of Internal Medicine I and Clinical Chemistry, University Hospital Heidelberg, Heidelberg, Germany

[9]Institute for Diabetes and Cancer (IDC) and Joint Heidelberg-IDC Translational Diabetes Program, Helmholtz Center Munich, Neuherberg, Germany

[10]These authors contributed equally

[11]These authors contributed equally

[12]Lead contact

*Correspondence:
Cesare Granata, Ph. D.
Institute for Clinical Diabetology
German Diabetes Center
Auf'm Hennekamp 65
40225 Düsseldorf
Germany
E-mail: Cesare.Granata@ddz.de
Tel.: +49 211 3382 229

Summary

Abnormal mitochondrial oxidative phosphorylation (OXPHOS) is key to the pathogenesis of several cardiometabolic diseases. The ketone bodies (KBs), β-hydroxybutyrate (HBA) and acetoacetate (ACA), are critical for tissue-specific energy metabolism under various pathophysiological conditions. However, robust methods quantifying their contribution as substrates for OXPHOS are lacking. Here, we first established comprehensive high-resolution respirometry protocols for assessing the differential contributions of HBA, ACA, and related ketolytic enzymes to OXPHOS in translational studies in mice and humans. We then utilized these protocols to demonstrate (i) organ-specific differences in KB-driven mitochondrial respiration in mice, (ii) lower KB-driven mitochondrial respiration in liver of humans with steatosis, skeletal muscle of humans with diabetes and in kidney of diet-induced obese mice, as well as (iii) higher mitochondrial KB utilization capacity in mouse and human failing heart. These results highlight organ-specific roles of KB metabolism in cardiometabolic diseases and shall help to identify novel targets in these pathways.

Keywords:

ketone bodies, mitochondrial respiration, diabetes, obesity, steatosis, heart failure, fasting, skeletal muscle, kidney, brain

Introduction

The ketone bodies (KBs), β-hydroxybutyrate (HBA) and acetoacetate (ACA), represent an energy source for all domains of life[1]. While they generally contribute less to mitochondrial oxidative phosphorylation (OXPHOS) than other substrates like glucose and non-esterified fatty acids, their contribution varies largely by organ and metabolic state[1,2]. Indeed, KBs are important reserve and thrifty substrates under specific physiological and pathophysiological conditions, such as fasting, heart failure (HF), and kidney disease[3-6].

In recent years, KBs have attracted growing research interest due to accumulating evidence for their therapeutic potential in various diseases, such as cardiovascular diseases, HF, cardiogenic shock[6-9], neurodegenerative disease[10], kidney diseases[11,12], hepatic steatosis[13], skeletal muscle atrophy[14], and cancer[15]. KBs not only serve as an alternative energy source, but also function as signaling metabolites[16], exerting complex effects to reduce oxidative stress, fibrosis and inflammation[11,17], as well as regulating DNA repair and autophagy[7].

Even though ATP generation is likely the most relevant aspect of KB degradation (ketolysis) in their role as alternative substrates[18], previous studies investigating KB metabolism did not quantify the actual contribution of KBs to mitochondrial OXPHOS capacity[19,20]. Instead, studies assessed surrogate parameters such as circulating KB concentrations, the protein abundance or activity of enzymes involved in KB metabolism, or tissue KB uptake, without evaluating KBs' direct contribution to ATP production in specific organs[21,22]. High-resolution respirometry (HRR) is the gold-standard technique for the assessment of mitochondrial OXPHOS capacity in different organs and cells[23,24]. Only one previous study tested KB substrates in HRR of heart and muscle tissue reporting that the KB contribution to mitochondrial OXPHOS capacity is minimal when other substrates are available[25]. Despite the interesting results, the aforementioned study did not assess the individual contribution to OXPHOS capacity of specific enzymes involved in ketolysis nor the direct contribution of KBs to OXPHOS capacity in other organs and disease states. Such studies would allow to compare the differential organ-specific contribution of KB metabolism under physiological and pathological conditions and thereby inform research aiming to generate novel therapeutic targets.

We hypothesized that KB oxidation is distinctly regulated in various human and mouse organs by different cardiometabolic diseases. To test this, we first established a set of novel and comprehensive Substrate-Uncoupler-Inhibitor Titration (SUIT) protocols enabling the assessment of the differential contribution of HBA, ACA, and related ketolytic enzymes on OXPHOS capacity, and the characterization of the interplay between the different enzymes involved in ketolysis. We subsequently utilized these protocols to explore KB-dependent mitochondrial respiration in different organs and species in the context of relevant pathologies linked to abnormal mitochondrial function[26], such as obesity, type 2

diabetes mellitus (T2D), HF, and metabolic dysfunction-associated steatotic liver disease (MASLD)[27], as well was during physiological fasting.

Results

Individual assessment of HBA- and ACA-supported respiration in various tissues

Prior to the development of a protocol reflecting the complete ketolytic pathway, we tested whether and to which extent the KBs, HBA and ACA, can drive respiration in various mouse and human organs individually, i.e., as independent substrates. This approach enabled us to test the kinetics of the main enzymes involved in ketolysis, β-hydroxybutyrate dehydrogenase (BDH1) and succinyl-CoA: 3-ketoacid (oxoacid) coenzyme A transferase (SCOT), both located in the mitochondrial matrix (Figure 1). To measure the first step of ketolysis, in which HBA is oxidized to ACA by BDH1 and which leads to reduction of NAD^+ to NADH, the involvement of the tricarboxylic acid (TCA) cycle is not necessary, as the NADH produced in this reaction enters the electron transport system (ETS) directly via CI (Figure 1). Accordingly, titration of HBA as a sole substrate at saturating ADP concentrations induced a concentration-dependent increase in oxygen flux (JO2) in permeabilized mouse heart, skeletal muscle (soleus), kidney cortex, and brain cortex, even without addition of malate (Figure 2A-D, respectively). This dose-dependent effect of HBA on JO_2 was confirmed in human permeabilized cardiac and skeletal muscle (vastus lateralis) fibers (Figure 2E and F, respectively). In mice, there was no difference in the Michaelis Menten constant (Km) of HBA (related to the enzyme BDH1, Figure 1, yellow shaded area) between all organs tested ($p > 0.05$; Figure 2G). The Km values for human heart and skeletal muscle are shown in Figure 2H. Since these organs were collected from different populations (heart from humans with HF and skeletal muscle from healthy humans), we refrained from comparing the Km values using statistical hypothesis testing, as their values might not portray the physiological differences in Km between these tissues within similar populations. To our knowledge, this is the first report quantifying HBA-supported respiration in the absence of malate or any other TCA cycle substrate, hence directly investigating the oxidative capacity of BDH1.

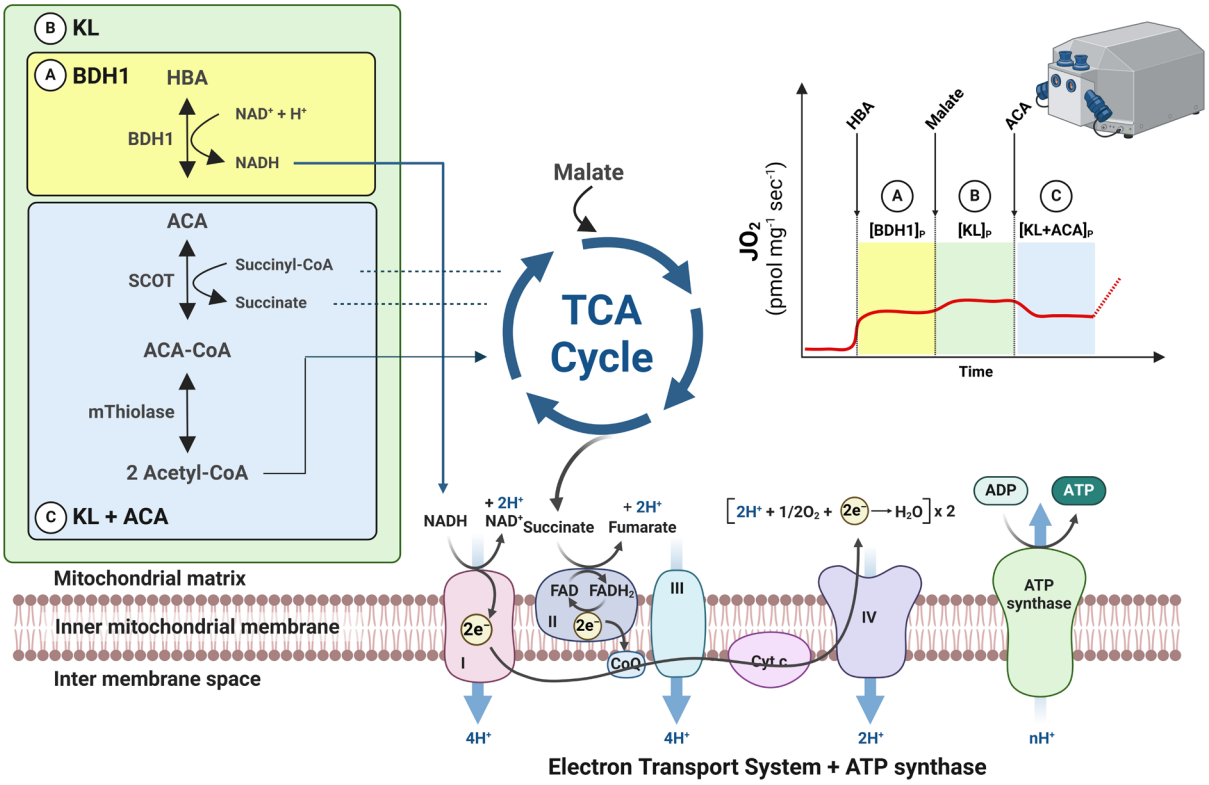

Figure 1: Pathways of ketone body-linked ATP generation by mitochondrial oxidative phosphorylation. Ketone body oxidation is initiated by addition of β-hydroxybutyrate (HBA; yellow shaded area, A); complete ketolysis is achieved by addition of malate (M; green shaded area, B); further addition of acetoacetate (ACA; blue shaded area, C) allows further insight into the interplay of the various enzymes involved in ketolysis (for a complete explanation, see further sections). ADP: adenosine diphosphate; ATP: adenosine triphosphate; BDH1: β-hydroxybutyrate dehydrogenase; CoA, coenzyme A; CoQ: coenzyme Q; e^-: electron; $FADH_2$: flavin adenine dinucleotide; H^+: proton; JO_2: oxygen flux; KL: ketolysis; NADH: nicotinamide adenine dinucleotide; SCOT: Succinyl-CoA: 3-ketoacid (oxoacid) coenzyme A transferase; TCA: tricarboxylic acid cycle. Figure generated using BioRender.com (Toronto, CA).

Unlike BDH1, the reaction catalyzed by SCOT, which converts ACA and succinyl-CoA to ACA-CoA and succinate, requires assistance from the TCA cycle (via addition of a TCA cycle substrate; e.g., malate) to provide sufficient concentrations of succinyl-CoA along with ACA (Figure 1). When titrated after malate at saturating ADP concentrations, ACA induced concentration-dependent JO2 increases in various mouse organs including heart, skeletal muscle (soleus), and kidney cortex (Figure 2I-K, respectively). In mouse brain cortex, no concentration of ACA resulted in increased JO2 (Figure 2L), even after isolation of brain cortex mitochondria to eliminate the possible interference of myelin presence on ACA availability (data not shown). This finding remains unexplained. Similar to mouse, addition of ACA in the presence of malate induced concentration-dependent JO_2 increases also in human heart and skeletal muscle (vastus lateralis) (Figure 2M and N, respectively). In mice, the Km for ACA, involving the enzymatic activity of both SCOT and the downstream enzyme mThiolase (Figure 1) was greater in kidney cortex compared to skeletal muscle and heart (Figure 2O). The Km values for ACA in human organs are shown in Figure 2P; no statistical hypothesis testing for these Km was performed for the same reasons mentioned above. Taken together, these results demonstrate that

individual KBs can be used separately to test their respective OXPHOS capacity in several human and mouse organs.

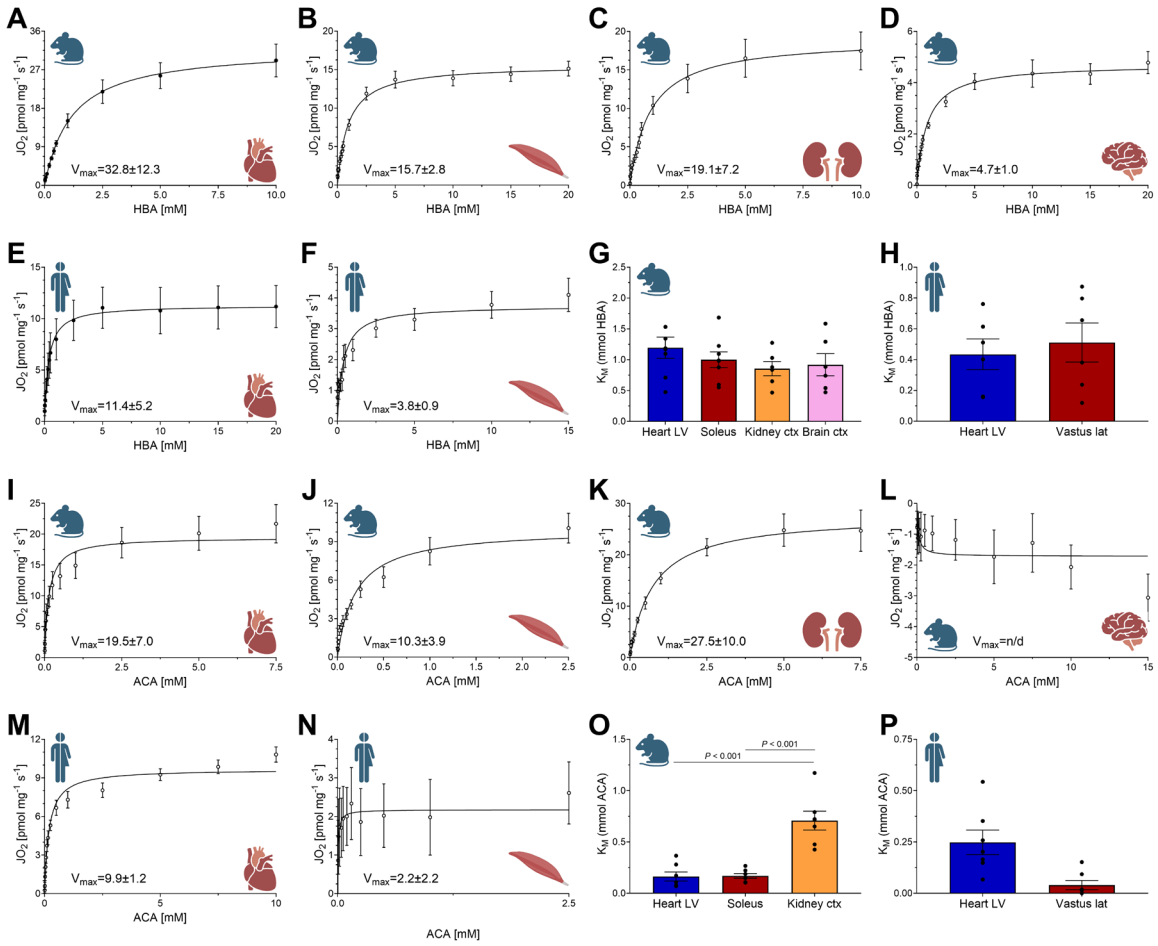

Figure 2: Michaelis-Menten kinetics for β-hydroxybutyrate (HBA) and acetoacetate (ACA) supported mitochondrial respiration in different mouse and human organs. Titration of HBA (A-D for mice, E, F for humans) and ACA (I-L for mice, M, N for humans) in heart left ventricle, skeletal muscle (soleus for mice; vastus lateralis for humans), kidney cortex, and brain cortex with non-linear regression fits based on the mean values according to the Michaelis Menten Equation. The Michaelis Menten constant (K_m) values for each individual sample are plotted in G (HBA mice), H (HBA humans), O (ACA mice), P (ACA humans), are presented as mean ± SEM, and were compared in mice, but not humans (see text), using Welch's ANOVA test (panel G and O). Maximal mitochondrial respiration (V_{max}) values are presented within each relevant panel and are expressed as [pmol O_2 mg^{-1} s^{-1}]. N=6-8 for mice. N=6-7 for humans. Ctx: cortex; JO_2: oxygen flux; lat: lateralis; LV: left ventricle; n/d: not determined. Icons obtained from BioRender.com.

Ketone body metabolism in the liver

Unlike other organs, where it is abundantly expressed, SCOT is not traceable in the liver, indicating the liver is not utilizing KBs to generate ATP *in vivo*[2]. Instead, the liver is the primary source of circulating KBs in humans for other organs through ketogenesis; this involves conversion of acetoacetyl-CoA to ACA, which is the rate limiting step of ketogenesis and it is catalyzed by hydroxymethylglutaryl-CoA synthase (HMGCS2)[28]. However, BDH1, the enzyme catalyzing the equilibrium reaction between HBA and ACA, is expressed in the liver to a relatively high extent[29]. Moreover, monocarboxylate transporter (MCT) 1 and other MCT proteins involved in the cellular transport of KBs are similarly present in hepatic

tissue as in other organs[1,30]. Thus, the liver should theoretically be able to use HBA as a substrate, even if degradation of ACA (to ACA-CoA and subsequently acetyl-CoA) cannot proceed further due to the lack of SCOT. To confirm this, we separately added HBA and ACA (the latter of which in the presence of malate) at saturating ADP concentrations in mouse liver, as we did for the other organs. The results show that addition of HBA as a sole substrate increased JO_2 dose-dependently, indicating that mouse liver can indeed oxidize HBA *ex-vivo* in what is likely to be a non-physiological direction (Figure 3A). To confirm that the JO_2 response to HBA measured in the liver stems from generation of ATP by the ETS, we subsequently added oligomycin, an inhibitor of ATP-synthase, followed by titration with carbonyl cyanide-p-trifluoromethoxyphenylhydrazone (FCCP), a widely used protonophore[23]. The marked decrease in JO_2 response following oligomycin injection and the pronounced increase measured after the addition of FCCP confirms the coupling between oxygen consumption at the level of CIV and ATP generation by ATP-synthase promoted by HBA at saturating ADP concentration (Figure S1). Furthermore, the marked decrease in JO_2 upon subsequent addition of rotenone, an inhibitor of CI[23], to values similar to those reached after final addition of Antimycin A, an inhibitor of CIII[23] (Figure S1), confirms that generation of ATP in the ETS in this experimental setting proceeds via NADH entry through CI, as portrayed in Figure 1.

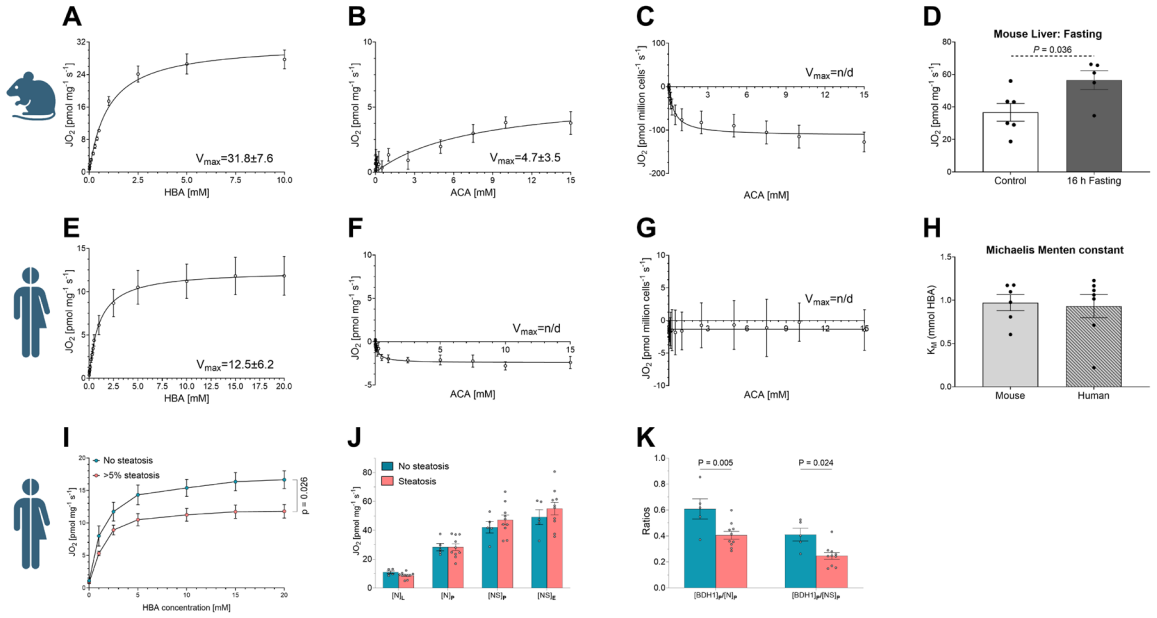

Figure 3: β-hydroxybutyrate (HBA)-driven mitochondrial respiration is altered in the human steatotic and mouse fasted liver. Titration of HBA (A) and acetoacetate (ACA, B) in mouse liver, and titration of HBA in mouse primary hepatocytes (C) with non-linear regression fits based on the mean values according to the Michaelis Menten equation. (D) Comparison of JO_2 following addition of HBA in the presence of saturating levels of ADP between mice after 16 h of fasting and mice with continuous access to normal chow. Titration of HBA (E) and ACA (F) in human liver, and titration of HBA in HepG2 cells (G) with non-linear regression fits based on the mean values according to the Michaelis Menten equation. (H) Michaelis Menten constant (K_m) values for each individual sample. I-K: Comparison of HBA-driven mitochondrial respiration in participants with and without hepatic steatosis (cutoff: histological hepatic fat content >5%). Repeated-measurements mixed-effects models with correction for multiple testing with the false discovery rate. A: n=6. B: n=7. C: n=7. D: n=6 vs. 5 for control vs. fasted, respectively. E, F: n=7. G: n=3. H: n=6 and 7 for mouse and human, respectively. I: n=5 vs. 11, and J, K: n=5 vs. 10 for non-steatosis vs. steatosis samples, respectively. Maximal mitochondrial respiration (V_{max}) values are presented within each

relevant panel and are expressed as [pmol O_2 mg^{-1} s^{-1}]. Panel D, H, J, and K are presented as mean ± SEM. $_E$: electron transport chain capacity (noncoupled) mitochondrial respiration state; JO_2: oxygen flux; $_L$: leak mitochondrial respiration state; N: NADH-linked substrates; n/d: not determined; $_P$: phosphorylating (coupled) mitochondrial respiration state; S: succinate-linked substrates. Icons obtained from BioRender.com.

Addition of ACA in the presence of malate, yielded minimal increases in JO_2 in mouse liver (Figure 3B). To confirm that this minimal increase in JO_2 could be attributed to hepatic cell types other than hepatocytes, we titrated ACA at saturating concentrations of malate and ADP in primary hepatocytes isolated from mouse liver. As expected, no concentration-dependent increase in JO_2 was detectable (Figure 3C). These results are consistent with recent findings demonstrating a hepatocyte-macrophage ketone shuttle, whereby liver macrophages have been shown to utilize ACA as fuel substrates in a mechanism coordinating a protective fibrogenic response to hepatic injury[31].

Fasting (including intermittent fasting and time-restricted feeding), is an established trigger of ketosis, which increases the preference for KBs as energy substrates in human tissues[19,32]. Beneficial effects of fasting in various pathological conditions have been at least partially attributed to increased ketonemia[33]. As a proof of concept, we compared HBA-driven respiration in mice fasted for 16 h with mice with continuous access to normal chow and found a greater JO_2 in livers of fasted mice (Figure 3D).

Titration of HBA at saturating ADP concentrations in human liver yielded a dose-dependent increase in JO_2, similar to mouse tissue, suggesting that also the human liver can indeed oxidize HBA *ex vivo* (Figure 3E). No JO_2 response was reported in human liver following ACA titration in the presence of saturating concentration of malate and ADP (Figure 3F). The inability to use ACA by human liver was also confirmed by a lack of response to ACA titration in a human hepatocyte cell line (HepG2 cells; Figure 3G). Taken together, our results indicate that, in the liver, HBA as a sole substrate yields JO_2 and Km values comparable to ketolytic organs in both mice and humans (Figure 3H, compare with Figure 2G and H). Conversely, ACA as an individual substrate even in the presence of malate, yields a minimal (mouse, Figure 3B) or not measurable (human, Figure 3F) dose-dependent response in JO_2, which stems from cells other than hepatocytes. Our data demonstrate that HBA oxidation can be quantified in the liver *ex vivo* using HRR. The resulting values are likely to simply represent the enzymatic activity of BDH1 in conjunction with that of cytosolic/mitochondrial transporters linked to ATP generation by OXPHOS, without involvement of the TCA cycle (Figure 1, yellow shaded area). However, whether BDH1 can operate in ketolytic fashion (oxidation of HBA to ACA) *in vivo* in the liver, which is primarily a ketogenic organ[2], remains to be determined.

Lower HBA-supported OXPHOS capacity in MASLD

Mitochondrial function plays an important role during the development and progression of human metabolic diseases. Hepatic OXPHOS capacity is upregulated in obesity and MASLD (mitochondrial plasticity) and fails during disease progression[34]. Based on the above findings, changes in the HBA-supported respiration state (termed $[BDH1]_P$) in the liver could be used as a readout of variations in hepatic KB metabolism in MASLD[26]. To test this, we compared $[BDH1]_P$ in obese humans with and without histologically confirmed MASLD (≥5% liver lipid content). Obese participants with and without MASLD had similar demographic and clinical characteristics (Table S1). Our data indicated lower hepatic $[BDH1]_P$ values at various HBA concentrations in obese participants with compared to those without MASLD (Figure 3I). Consistent with previous reports[34], mitochondrial respiration induced by substrates entering the ETS via CI (N pathway) or CI+II combined (NS pathway) was not different between steatotic and non-steatotic hepatic tissue in this obese cohort (Figure 3J). As a result, relative to maximal OXPHOS capacity through the N pathway (which is particularly relevant in this case because the reducing equivalents generated by HBA in the liver enter the ETS only via CI), $[BDH1]_P$ was lower in steatotic compared to non-steatotic tissue (Figure 3K). Similar differences were seen when normalizing by the NS pathway (Figure 3K). Of note, given the liver's ketogenic nature, the JO_2 values measured in this experiment likely reflect a non-physiological direction (HBA oxidation to ACA). Therefore, this result represents a quantification of the enzymatic activity of hepatic BDH1 in conjunction with that of mitochondrial and cellular transporters and the respiratory chain enzymes, which can be interpreted in the direction of both ketolysis and ketogenesis.

Combined ketone body SUIT protocol reveals organ-specific differences in mice

To determine the complete contribution of ketolysis to OXPHOS and the interplay between the different ketolytic enzymes, we developed a novel combined KB SUIT protocol consisting of the sequential addition of HBA (to assess $[BDH1]_P$; Figure 1, yellow shaded area), malate (to assess complete ketolysis, $[KL]_P$; Figure 1, green shaded area), and ACA (either titrated stepwise or added in a single injection, to assess potential differences in the activity of distinct ketolytic enzymes $[KL+ACA]_P$; Figure 1, blue shaded area). For a detailed explanation of this protocol, the reader is referred to the Methods section. Owing to the inability of hepatocytes to undergo ketolysis due to the lack of SCOT [2], our combined KB SUIT protocol is unsuitable for hepatic tissue, as the respiratory states $[KL]_P$ and $[KL+ACA]_P$ cannot be achieved, so we limited this analysis to the four ketolytic mouse organs tested in this study. Renal cortex presented with the greatest KB-driven OXPHOS capacity in all three respiratory states, followed by the heart and skeletal muscle (Figure 4A). Brain cortex yielded the lowest values throughout (Figure 4A). These findings are consistent with previous literature comparing the gene expression and activity of ketolytic enzymes, as well as these organs' KB uptake[2,4,35-37].

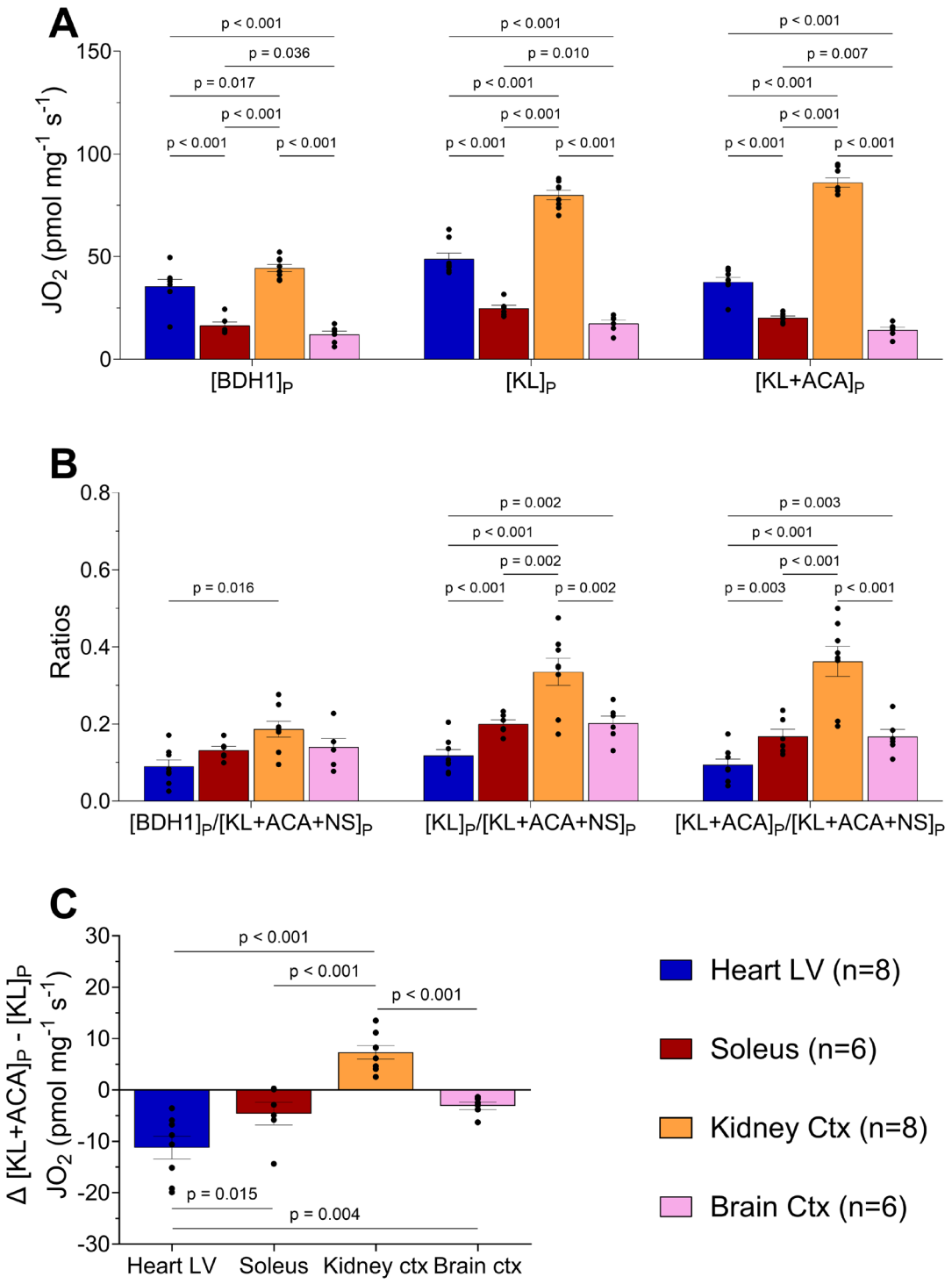

Figure 4: Combined ketone body (KB) mitochondrial respiration protocol in various mouse organs. (A) Mitochondrial respiration (JO_2) readouts from the combined KB respirometry protocol, as well as (B) ratios between β-hydroxybutyrate 1 phosphorylation ($[BDH1]_P$), ketolysis phosphorylation ($[KL]_P$), ketolysis plus acetoacetate (ACA) phosphorylation ($[KL+ACA]_P$) and maximal OXPHOS capacity ($[KL+ACA+NS]_P$) obtained from experiments shown in Figure S2 in mouse heart left ventricle (LV), soleus, kidney cortex (ctx) and brain cortex. (C) Calculated difference between $[KL+ACA]_P$ and $[KL]_P$ following 1 mM ACA addition for mouse heart LV, soleus, kidney cortex, and brain cortex. N=6-8 per figure. All panels: mean ± SEM. A, B: Repeated-measurements mixed-effects model (REML) with correction for multiple testing with the false discovery rate. C: One-way ANOVA with correction for multiple testing with the false discovery rate. JO_2: oxygen flux; N: NADH-linked substrates; $_P$: phosphorylating (coupled) mitochondrial respiration state; S: succinate-linked substrates.

To gain further insight into the contribution of KBs metabolism to maximal OXPHOS capacity, we calculated the ratios between the three states of KB-linked mitochondrial respiration and the maximal OXPHOS capacity achieved following subsequent activation of the NS pathway (Figure S2). Renal cortex presented once again with the greatest relative contribution of KBs to maximal OXPHOS capacity of all the organs tested (Figure 4B), consistent with previous findings showing that various cell types within the kidney rely on KBs as preferred substrates[5]. Conversely, the relative contribution of complete ketolysis ($[KL]_P$) to maximal OXPHOS capacity was lower in the heart compared to all other organs tested (Figure 4B). This result was likely driven by the much greater maximal OXPHOS capacity ($[KL+ACA+NS]_P$) of the left ventricular myocardium compared to the other organs (Figure S2), which is in line with previous studies[38]. Despite the lowest absolute values (Figure 4A), the relative contribution of $[BDH1]_P$ to maximal OXPHOS capacity for brain cortex was not different to that of the other organs tested and $[KL]_P$ was second highest after the kidney (Figure 4B). These findings are consistent with the significant role played by KBs as alternative substrates to glucose in the brain[39].

Addition of 1 mM ACA resulted in a JO_2 decrease, suggesting a product-induced inhibition of the equilibrium reaction catalyzed by BDH1 (Le Chatelier's principle), in all organs tested with the exception of the kidney, for which JO_2 increased (Figure 4C). This suggests that the reaction catalyzed by BDH1 is the rate-limiting step of ketolysis in C57BL/6J female mouse kidney cortex, as SCOT/mThiolase presents with a "reserve capacity" for ACA conversion to acetyl CoA. This is a novel finding as previous studies reported SCOT as the rate limiting enzyme of ketolysis[4,40,41].

To further characterize the KBs contribution to OXPHOS capacity in different human and mouse organs we applied our novel respirometry protocols to cohorts with distinct pathophysiological states that are thought to be associated with altered KB metabolism.

Greater ketone body contribution to OXPHOS capacity in the failing heart

Employing our combined KB SUIT protocol in ventricular myocardium to identify their role as mitochondrial substrates in the setting of HF, we compared humans with advanced HF with humans after heart transplantation without HF (controls), who differed in cardiac function but not demographic characteristics (Table S2). Our results indicate no differences in JO_2 between groups in any of the KB-linked respiratory states assessed ($[BDH1]_P$, $[KL]_P$, and $[KL+ACA]_P$; (Figure 5A). In contrast, the respiratory states $[F]_P$, $[FN]_P$, and $[FNS]_P$ were markedly lower in the HF group (Figure 5B), consistent with previous observations by our group and others[42,43]. As a result, the relative contribution of KB metabolism to maximal OXPHOS capacity ($[FNS]_P$) was greater in humans with HF compared to controls in two KB-linked respiratory states ($[KL]_P$, $[KL+ACA]_P$ and followed a similar trend in the third one ($[BDH1]_P$; $p=0.085$) (Figure 5C). Moreover, further addition of ACA resulted in a decrease in JO_2, indicating a product-induced inhibition of the reaction catalyzed by BDH1, only in the control group,

so that the Δ[KL+ACA]$_P$-[KL]$_P$ value was lower in control compared to HF participants (Figure 5D). Taken together, these results demonstrate that preservation of KB-linked respiration in HF results in a greater reliance of the failing heart on ketolysis, as its ability to generate ATP via KB metabolism is maintained whereas that linked to the FNS pathway is greatly diminished.

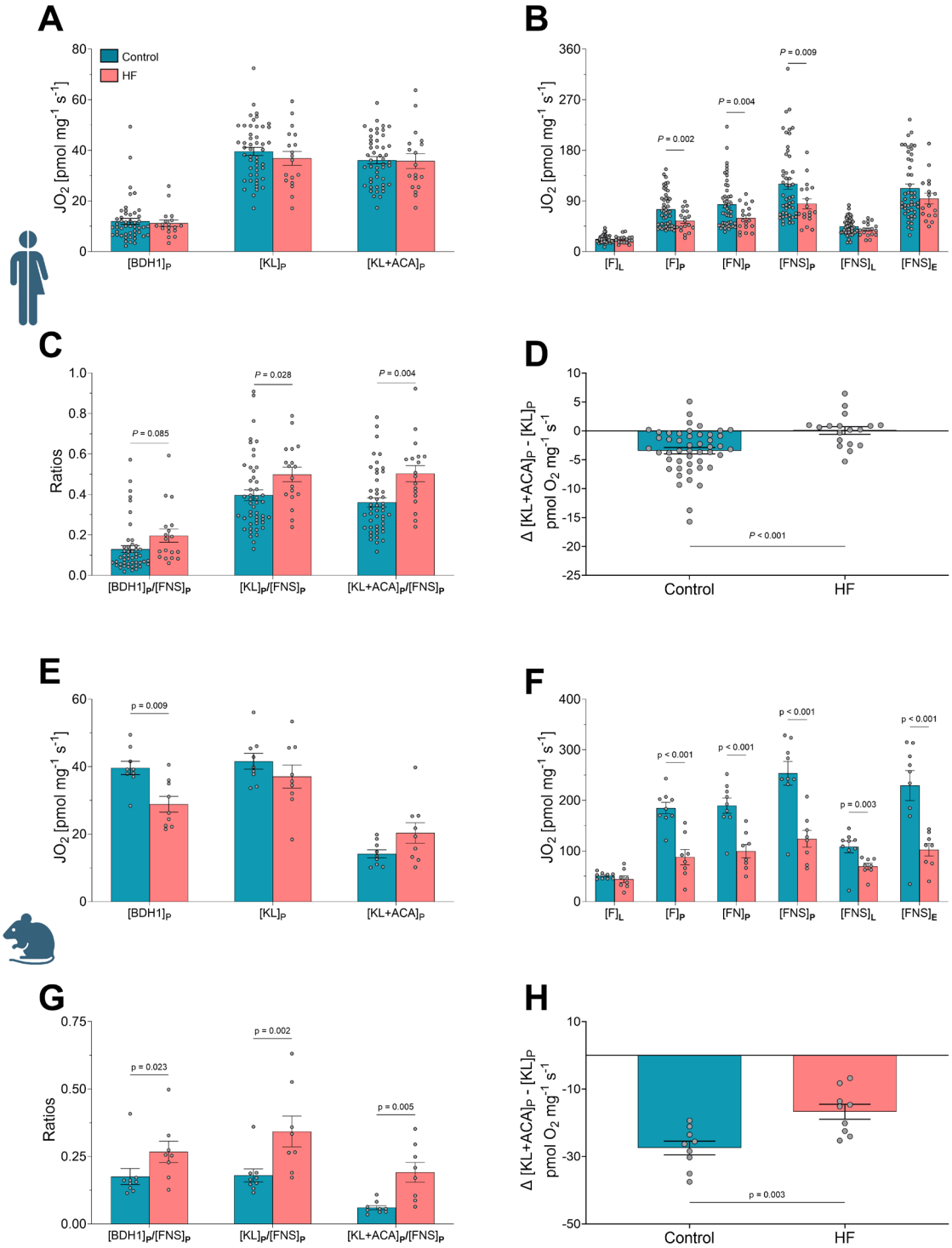

Figure 5: Ketone body-linked respiration in the failing and non-failing human and mouse heart. Mitochondrial respiration (JO_2) of permeabilized ventricular myocardium from participants with heart failure (HF) versus heart transplant recipients without HF undergoing routine endomyocardial biopsy (Control group), obtained with (A) the combined ketone body (KB) and (B) the fatty acid oxidation, NADH, and succinate combined (FNS) pathway mitochondrial respiration protocols. (C) Relative

contribution of the different respiratory states of KB-linked versus maximal FNS-linked phosphorylating mitochondrial respiration. (D) Effect of addition of 5 mM acetoacetate (ACA) on JO_2 ($\Delta[KL+ACA]_P$-$[KL]_P$). Panel E to H represent the same analyses as A to D, respectively, performed in permeabilized ventricular myocardium of mice with HF after ischemia (HF) versus control mice (Control) with 7.5 mM ACA. A, B, C: Repeated-measurements mixed-effects model with correction for multiple testing with the false discovery rate. D: Mann-Whitney test. A-D: n=47-48 (control) versus 17-18 (HF). E, F, G: Repeated-measurements mixed-effects model with correction for multiple testing with the false discovery rate. H: Unpaired t-test. E-H n=9 (control) versus 8-9 (HF). Data are mean ± SEM. BDH1: β-hydroxybutyrate 1; $_E$: electron transport chain capacity (noncoupled) mitochondrial respiration state; JO_2: oxygen flux; KL: ketolysis; $_L$: leak mitochondrial respiration state; $_P$: phosphorylating (coupled) mitochondrial respiration state. Icons obtained from BioRender.com.

To confirm these findings, we used a mouse model of ischemic HF. We performed a similar assessment of KB metabolism in ventricular myocardium of mice with HF induced by myocardial ischemia without reperfusion (HF)[44] versus healthy mice (control) (Table S3). With the exception of $[BDH1]_P$, which was greater in controls compared to HF mice, the other KB-linked respiratory states assessed were not different between the groups, mirroring the human results (Figure 5E). Similar to the human data, the three phosphorylating respiratory states $[F]_P$, $[FN]_P$, and $[FNS]_P$ were lower in HF versus control mice (Figure 5F). Also similar to our human results, the relative contribution of KBs to maximal OXPHOS capacity ($[FNS]_P$) was greater in HF mice for all KB-dependent respiratory states (Figure 5G). Finally, addition of ACA lowered the JO_2 in both groups (both $p<0.001$), such that the $\Delta[KL+ACA]_P$-$[KL]_P$ values were lower in control compared to HF mice (Figure 5H), similar to the human cohort. The difference in $[BDH1]_P$ between humans and mice may be linked to a greater impairment of the N pathway in HF mice (-53% *vs.* control) than in HF humans (-27% *vs.* control) and was partially rescued after normalization to maximal OXPHOS (Figure 5G). Taken together, the studies in mice largely mirror those in humans, highlighting the greater reliance on KBs as myocardial mitochondrial substrates in HF (compare Figure 5C and G).

Lower KB-dependent OXPHOS capacity in the type 2-diabetic skeletal muscle

Owing to the lower OXPHOS capacity in skeletal muscle of T2D than in glucose tolerant humans[26,45], we aimed to investigate if the capacity to utilize KBs for ATP production is also reduced in skeletal muscle of humans with T2D. Study participants with and without T2D, as defined by current guidelines[46], did not differ with respect to demographic characteristics such as age, sex or body mass index (Table S4). Using our combined KB SUIT protocol, we detected lower KB-linked OXPHOS capacity in humans with T2D in the $[KL]_P$ and the $[KL+ACA]_P$ states, and a similar albeit not statistically significant trend in the $[BDH1]_P$ state (Figure 6A). Similar to Boushel et al.[47], but different from other previous studies[48-51], we did not detect a difference in mitochondrial OXPHOS capacity between humans with and without T2D in the NS pathway (Figure 6B). However, the relative contribution of KBs to maximal OXPHOS capacity was ~70-140% greater in the glucose tolerant participants compared to those with T2D in all three KB-linked respiration states (Figure 6C). Participants with T2D responded with decreased respiration to the addition of ACA, but without a difference in $\Delta[KL+ACA]_P$-$[KL]_P$ between groups ($p=0.103$, Figure 6D). Finally, lower insulin sensitivity, as assessed using the oral glucose insulin

sensitivity (OGIS) index[52], was associated with a lower relative KB contribution to maximal OXPHOS capacity expressed as $[KL]_P/[NS]_P$ and presented a similar trend with $[BDH1]_P/[NS]_P$ (Figure S3). Overall, these findings indicate a reduced ability of skeletal muscle mitochondria to utilize KBs as a substrate to generate ATP through OXPHOS in individuals with T2D as compared to those without T2D, supporting the concept of impaired metabolic flexibility in human skeletal muscle with T2D[26,45].

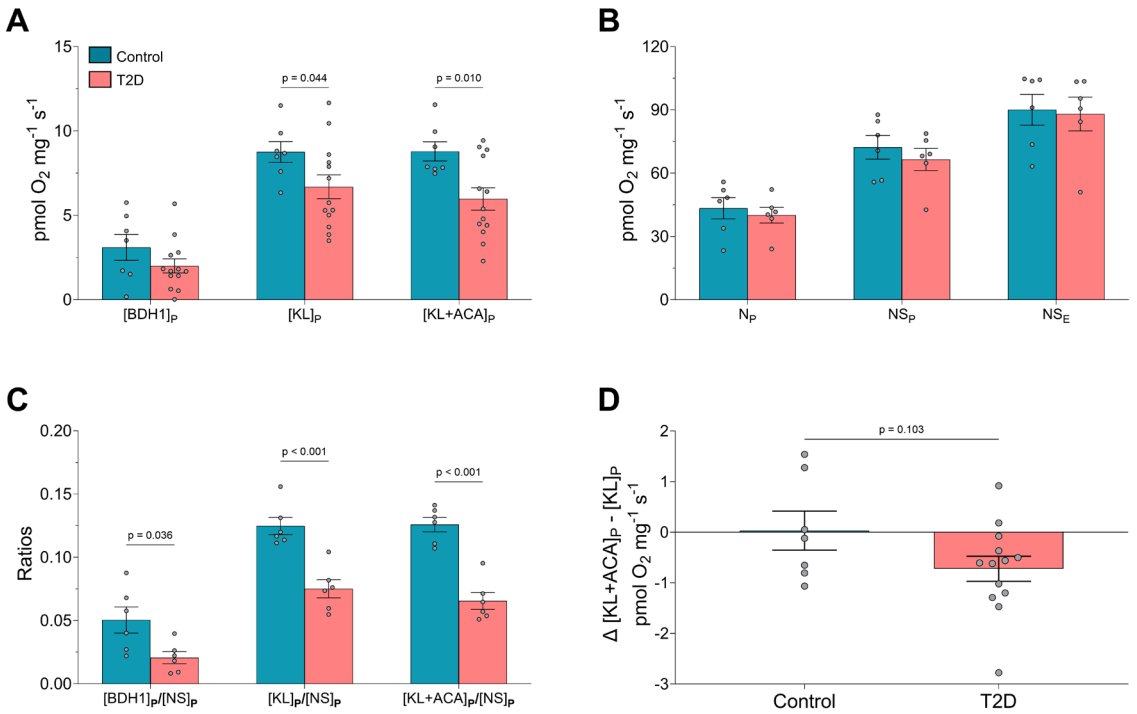

Figure 6: Ketone body-dependent mitochondrial respiration in skeletal muscle of humans with type 2 diabetes mellitus (T2D) versus controls. Mitochondrial respiration (JO_2) in permeabilized skeletal muscle (vastus lateralis) fibers obtained with (A) the combined ketone body and (B) the NADH and succinate combined (NS) pathway mitochondrial respiration protocols. (C) Relative contribution of the different respiratory states of KB-linked versus maximal NS-linked mitochondrial respiration. (D) Effect of addition of 1 mM acetoacetate (ACA) on JO_2 ($\Delta[KL+ACA]_P$-$[KL]_P$). A, D: N=7 vs. 13. B, C: N=6 vs. 6. A-C: Repeated-measurements mixed-effects model with correction for multiple testing with the false discovery rate [53]. D: Unpaired t-test. Data are mean ± SEM. BDH1: β-hydroxybutyrate 1; $_E$: electron transport chain capacity (noncoupled) mitochondrial respiration state; JO_2: oxygen flux; KL: ketolysis; $_L$: leak mitochondrial respiration state; N: NADH-linked substrates; $_P$: phosphorylating (coupled) mitochondrial respiration state; S: succinate-linked substrates.

Alterations of KB-dependent OXPHOS capacity in kidney cortex

Not only T2D, but obesity is already associated with altered kidney function; this include glomerular hyperfiltration leading to glomerular hypertrophy, ectopic renal lipid accumulation promoting insulin resistance of the podocyte and other maladaptive responses, and severe alterations in renal metabolic flux including dysregulation of fatty acid metabolism driving renal inflammation, oxidative stress, and fibrosis[5,54,55]. Most important for the scope of our research, increasing evidence suggests that mitochondrial alterations are associated with kidney disease in both the nondiabetic a diabetic setting, and that altered renal mitochondrial function is a pathological mediator of kidney disease[5,55]. Given the above background, we sought to investigate if renal KB-driven mitochondrial respiration is also

affected by obesity and insulin resistance. In the absence of fresh human kidney cortex, we utilized our combined KB respirometry protocol to investigate potential alterations in KB-linked mitochondrial respiration in the kidney cortex of a diet-induced obese (DIO) C57BL/6J mouse model reflecting obesity-related prediabetes[56]. When the dietary fat content is 60%, like in the present study, this mouse model has been shown to develop glomerular hypertrophy and glomerulosclerosis[57], as well as albuminuria and renal mesangial matrix expansion[58], which are hallmarks of kidney disease[5]. Mouse characteristics are presented in Table S5.

Absolute KB-linked respiration was lower in DIO mice compared to controls for all KB respiratory states (Figure 7A), suggesting that these metabolic conditions reduced the ability of renal cortex to generate ATP from KBs. No difference between groups was reported following the subsequent addition of NS-pathway substrates ($[KL+ACA+NS]_P$: 237.56 ± 45.26 and 240.46 ± 71.86 pmol s^{-1} mg^{-1} for control and DIO mice, respectively; p=0.910, unpaired Welch's t test). The relative contribution of KB-driven respiratory states to maximal OXPHOS capacity was also reduced in DIO *vs.* controls for all KB respiratory states (Figure 7B). The decrease in mitochondrial respiration after addition of ACA was not different between groups (Figure 7C). This also indicates that the "reserve capacity" of SCOT/mThiolase observed in renal cortex of female mice in Figure 4C was not present in older (35 week) male mice (Figure 7C), which may stem from sex- and/or age-driven differences in of renal KB metabolism. Taken together, these findings demonstrate that obesity-related prediabetes results in a reduced ability of renal mitochondria to utilize KBs for ATP production by OXPHOS.

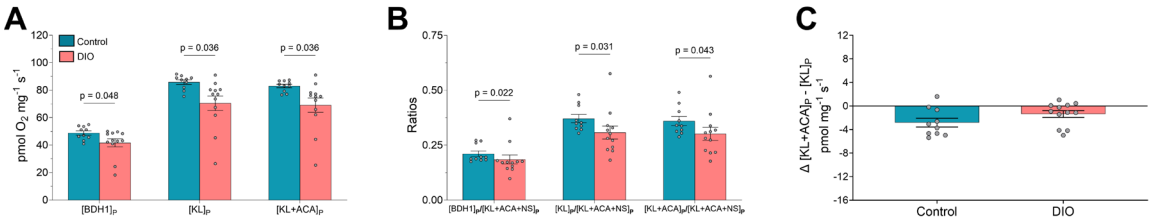

Figure 7: KB-driven oxygen flux (JO_2) in kidney cortex of 35-week-old diet induced obesity (DIO) versus controls C57BL/6J male mice. A, B: Multiple Mann-Whitney-Tests, corrected for multiple testing with the Holm-Šídák method. C: Unpaired t-Test. N=10 vs. 12. Data are mean ± SEM. ACA: acetoacetate; BDH1: β-hydroxybutyrate 1; KL: ketolysis; N: NADH-linked substrates; P: phosphorylating (coupled) mitochondrial respiration state; S: succinate-linked substrates.

Discussion

In the present study, we devised targeted HRR protocols to obtain a comprehensive and sensitive readout of mitochondrial KB utilization for energy supply. These protocols, which have a wide applicability range extending to various tissues and species, enabled us to detect novel tissue-specific features of mitochondrial KB utilization in the presence of distinct cardiometabolic diseases.

While the liver is primarily ketogenic and the main source of circulating KBs in humans and mice[28], evidence exists about the ability of specific liver cells (macrophages) to utilize KBs as fuel substrates[31]. Despite the lack of SCOT in hepatocytes[2], the presence of BDH1 and other proteins involved in the cellular transport of KBs[1,30] lends to the hypothesis that HBA could be utilized as a fuel substrate by the liver. Using our HRR protocols we verified that – at least *ex vivo* – the first step of ketolysis (conversion of HBA to ACA) can also take place in hepatic tissue, confirming the above hypothesis. In addition, by using a designated HRR protocol we subsequently showed in mice that HBA-supported respiration in the liver is greater in the fasted state. Finally, we demonstrated that in obese humans with hepatic steatosis HBA-supported mitochondrial respiration is significantly reduced compared with obese individuals without hepatic steatosis, both in absolute and relative terms. Even if the clinical relevance of HBA oxidation in the liver *ex vivo* remains mostly unknown, the decrease in $[BDH1]_P$ in the presence of maintained CI- and CII-linked OXPHOS capacity could indicate either (i) a state of impaired ketogenesis, suggesting that $[BDH1]_P$ can be utilized as a marker of hepatic functional alterations and inadequate mitochondrial adaptations in hepatic steatosis, and/or (ii) a reduced ability of liver mitochondria to generate energy from HBA (limited to the first step of ketolysis catalyzed by BDH1), representative of impaired metabolic flexibility[59]. Both, mitochondrial alterations and metabolic inflexibility are increasingly recognized as hallmarks of MASLD[59-61]. Future research should therefore investigate if the liver indeed oxidizes HBA also *in vivo* and if this is altered during progression of MASLD. Such studies will have the potential to identify novel pathways to target the not yet fully met need to reverse liver fibrosis.

Previous research reported alterations of KB metabolism in humans with and animal models of HF[6,8,22,62]. Although accumulating evidence indicates a therapeutic role for KBs in cardiovascular diseases, HF, and even cardiogenic shock[6-9,63], there remains uncertainty as to whether the KBs' cardioprotective effects can be attributed to their role as mitochondrial substrates or should be ascribed to other KBs' functions, such as their role as signaling molecules[64,65]. Our data demonstrated that in the failing heart myocardial mitochondria maintain their capacity to utilize KBs for ATP generation despite a compromised ability to generate energy via other pathways, such as the degradation of fatty acids ($[F]_P$), or that of substrates of the N ($[FN]_P$) and S ($[FNS]_P$) pathway. This resulted in a greater relative contribution of KB metabolism to energy supply in the human failing heart compared to controls. Whether this is the result of the compromised activity of enzymes involved in the FNS pathways induced by HF or relates to a different metabolic landscape resulting in greater circulating KBs in HF, remains to be determined. Taken together, our findings lend further support to approaches of KB supplementation in humans with HF[63].

Skeletal muscle of individuals with insulin resistance or T2D features alterations in mitochondrial quality control processes, content, and respiratory function resulting in impaired mitochondrial flexibility[26,66], which in turn leads to compromised skeletal muscle mitochondrial plasticity[45]. There are discrepancies related to studies investigating changes in mitochondrial respiration in skeletal muscle of humans with T2D when this is stimulated with substrates of the NS (or FNS) pathway; while the majority of the available literature has shown that T2D is associated with a reduction in mitochondrial OXPHOS capacity[48-51], a lack of change has also been reported[47], as also indicated by our current findings. However, the present study is the first to report a decrease in KB-linked mitochondrial OXPHOS capacity in T2D skeletal muscle. This is in line with findings from pioneering research demonstrating that KB uptake capacity is reduced in the skeletal muscle of rats with streptozotocin-induced diabetes[67,68]. In addition, our studies showed that also skeletal muscle of humans with T2D exhibits a marked decrease in the relative contribution of KB metabolism to energy production, which associated with lower insulin sensitivity supporting a role of KBs in myocellular insulin resistance. Although the contribution of KB-linked mitochondrial respiration is minimal compared to classic NS pathway substrates in human skeletal muscle, as previously reported[25], the whole-body contribution remains physiologically relevant, due to the large contribution of skeletal muscle to total body mass[4,25]. Therefore, targeting skeletal muscle may be particularly important in the clinical setting, as pharmacological interventions aimed at improving KB-metabolism in this organ may be a suitable and valuable option to improve the metabolic health of individuals at risk of or with overt diabetes.

KB metabolism plays a central role in the kidney, due to its almost unique ability to both produce and utilize KBs, and to the role of KBs as preferred substrates in normal physiological conditions or as readily available substrates during challenging or under fasted conditions[5]. Obesity induces a host of renal mitochondrial alterations which hampers the kidney's ability to carry out its physiological functions[5,54,55]. Using designated HRR protocols, we demonstrated that diet-induced obesity results in a decrease in KB-linked OXPHOS capacity in the kidney cortex of male mice, even if the capacity to generate ATP via substrates of the NS pathway remains unchanged. The decrease in BDH1-linked mitochondrial respiration in our DIO mice is consistent with previous findings in the kidney cortex of diabetic rats demonstrating that severe hyperglycemia is associated with significantly lower BDH1 protein content than normoglycemia, and that BDH1 protein content presents with a strong and positive correlation with plasma cystatin C[69], a marker of renal function[11]. The present findings support the concept of impaired metabolic flexibility in the diabetic kidney cortex[70], which in our study presented as early as in the obese prediabetic state. This suggests that obesity-induced derangement of renal KB metabolism may represent an early adaptation that is associated with the proven dysregulation of fatty acid metabolism, which is part of broader alterations in the metabolic landscape in the obese kidney[55]. Moreover, animal experiments have shown diabetes-induced accumulation of

KBs in the kidney parenchyma[5,71], and that the kidneys' KB intake remains unchanged in diabetes, indicative of increased endogenous ketogenesis in the diabetic kidney[5].

Advantages of comprehensive HRR in studies of KB metabolism

One of the main advantages of utilizing HRR to determine KB-linked mitochondrial respiration is that the readouts reflect the integrated functionality of the various processes involved in mitochondrial KB metabolism, including KB uptake into mitochondria, mitochondrial ketolysis, transport of reducing equivalents to the OXPHOS system, and the final generation of ATP in the ETS. As a results, our HRR readouts provide a sensitive, comprehensive, and accurate assessment of these processes as a whole, *ex vivo*. This *ex vivo* setting offers a much closer representation of *in vivo* KBs metabolism than other currently used spot readouts, such as determination of a single enzyme content or activity, the amount of circulating KBs, or individual KBs uptake by specific organs, as HRR is performed on a fully functional mitochondrial system[19,20,22,25]. In addition, our HRR protocols allow for the determination of mitochondrial respiratory function in whole-tissue samples without the need to perform mitochondrial isolation, which has been shown to (i) result in the disruption of mitochondrial structure and function and (ii) need larger tissue amounts[24,72].

Beyond the only previous report using KBs as respiratory substrates[25], our present work confirms their applicability as HRR substrates and provides several novel findings. i) The initial step of ketolysis catalyzed by BDH1 can be directly quantified in HRR with a protocol distinguishing HBA-induced TCA cycle-dependent from TCA cycle-independent OXPHOS capacity. This modification to the only previously published protocol[25] allows to determine the individual contribution to ATP generation by the reaction catalyzed by BDH1 (before addition of malate) regardless of its interaction with the TCA cycle ($[BDH1]_P$), and a readout for complete ketolysis (after malate addition; $[KL]_P$). ii) The interplay between the different enzymes involved in ketolysis (e.g., the presence of an enzyme with excess capacity or one whose activity is rate-limiting) can be determined with our combined KB SUIT protocol via ACA bolus addition or titrations. iii) By integrating findings from our combined KB SUIT protocol and the classic NS (or FNS) pathway protocol, our approach enabled the characterization of the relative contribution of KB metabolism to maximal OXPHOS capacity in several pathophysiological states in different species and organs. Correspondingly, this is the first report investigating and mapping the contribution to mitochondrial OXPHOS capacity of different enzymes involved in ketolysis in the human heart, skeletal muscle, and liver, as well as the same three organs, the kidney, and the brain in mice.

Limitations

While we tested our protocols in various organs as well as in both mice and humans, several other animal models of disease and human tissues require further studies to confirm the general feasibility

of these novel protocols. Consequently, other experimental models or human populations might need adaption of the proposed concentrations and titrations amounts described in these protocols. Furthermore, human studies always suffer from limitations such as pharmacological treatments and comorbidities of the control group; this was the case in our human heart cohorts, yet, the large well-characterized control group is also a specific aspect of this study[73,74]. In addition, access to functioning heart and liver tissue of humans is limited, which prevented us from conducting further analyses. However, both the HF and MASLD cohorts are unique, as they also offered data on several other aspects of mitochondrial metabolism in human hearts[75,76] and livers[34,77].

Conclusions

In conclusion, we devised novel HRR protocols to assess KB metabolism, demonstrating an organ-specific response to different KBs. Furthermore, our work highlighted, that distinct pathophysiological states such as hepatic steatosis, HF, T2D, obesity, and fasting, result in distinct alterations of mitochondrial KB metabolism. Despite their subordinate role as mitochondrial fuel in physiological settings for most organs, the use of KBs for ATP production via oxidative phosphorylation can now be assessed *ex vivo* across various pathophysiological settings with these HRR protocols. This will help filling the evident gap of previous literature that was limited to the assessment of single aspects of KB metabolism. Translationally, our findings suggest that in certain cardiometabolic conditions (such as HF), increasing the availability of KB substrates could represent a valuable therapeutic strategy, as in the failing heart the capacity to utilize KBs for ATP generation is maintained. Conversely, in other pathophysiological conditions such as the diabetic muscle, the steatotic liver, or the obese kidney, instead of increasing ketonemia, targeting tissue-specific KB OXPHOS capacity and metabolic flexibility may be a promising therapeutic approach.

Data availability

The datasets used and/or analyzed during the current study are available from the corresponding author upon request.

Acknowledgements

We would like to thank Julius Borger, Fariba Zivehe, Lea Zimmermann, Olga Dürrschmidt, Alexandra Stein, and Michelle Reina do Fundo for their help in mouse and tissue handling, and for performing respirometry. We acknowledge the support of the Susanne-Bunnenberg-Stiftung at the Düsseldorf Heart Center. We acknowledge the support of the GDS. The German Diabetes Study (GDS) Group consists of M. Roden (speaker), H. Al-Hasani, B. Belgardt, G. Bönhof, G. Geerling, C. Herder, A. Icks, K. Jandeleit-Dahm, J. Kotzka, O. Kuß, E. Lammert, W. Rathmann, S. Schlesinger, V. Schrauwen-Hinderling, S. Trenkamp, R. Wagner and their co-workers who are responsible for the design and conduct of the GDS.

Funding

This work is supported by grants from the German Research Foundation (Deutsche Forschungsgemeinschaft; DFG) (CRC1116, grant number 236177352) and by the German Diabetes Center (DDZ), which is funded by the German Federal Ministry of Health (BMG) and the Ministry of Culture and Science of the State of North Rhine-Westphalia (MKW NRW) and receives grants by the German Center for Diabetes Research (DZD e.V.), which is funded by the German Federal Ministry of Education and Research (BMBF) and by the MKW NRW. The work of EZ is supported by grants from the DFG (numbers 527448911, 493659010), the German Heart Foundation (F/22/18) and from the German Diabetes Society (DDG) (Menarini research grant 2020). The work of MR is further supported by grants from the European Community (HORIZON-HLTH-2022-STAYHLTH-02-01: Panel A) to the INTERCEPT-T2D consortium and the Schmutzler-Stiftung to the DDZ.

Author contributions

EZ, SP, AP, JS, MR, and CG contributed to conceptualization of the project. EZ, SP, JWS, RR, and CG contributed with performing the experiments. EZ, SP, JWS, DS, MS, SK, VB, BD, RR, AC, HA-H, HA, UB, AL, AP, MK, RaW, RoW, JS, MR, and CG contributed to sample acquisition. EZ, JWS, SP, and CG contributed to data analysis and figure making. EZ, SP, and CG contributed to writing of the first draft. EZ, JS, RW, MR contributed to funding acquisition. All authors reviewed the manuscript critically and approved the final version.

Declaration of interests

AP receives research funding from Abiomed outside of this work. RaW is employed by Abiomed. RoW reports lecture fees from Novo Nordisk, Sanofi-Aventis, Boehringer Ingelheim and Eli Lilly, and served

on the advisory board for Akcea Therapeutics, Daiichi Sankyo, Sanofi-Aventis, Eli Lilly, and NovoNordisk. MR is currently on scientific advisory boards of Astra Zeneca, Boehringer Ingelheim, Echosens, Eli Lilly, Madrigal, Merck-MSD, Novo Nordisk, and Target RWE, and has received support for investigator-initiated studies from Boehringer Ingelheim, Novo Nordisk and Nutricia/Danone. The other authors declare no competing interests.

Supplemental information

Document S1. Figures S1–S4 and Tables S1-S7

Materials and Methods

Laboratory mice and tissue harvest

All mouse procedures were approved by Animal Experimental Committee of the local government "Landesamt für Natur, Umwelt und Verbraucherschutz Nordrhein-Westfalen" (LANUV) and performed in accordance with the European Convention for the Protection of Vertebrate Animals used for Experimental and other Scientific Purposes (Council of Europe Treaty Series No. 123) and 2010/63/EU.

Protocol validation in mice. Mice used for protocol validation, generation of K_M plots (Figure 2A-D, G, I-L, and O; Figure 3A-C, and H) characterization of our combined KB SUIT protocol (Figure 4A-C), and Figures S1, S2, and S4D) were female wildtype C57BL/6J mice aged 16-26 weeks. Mice were fed with a standard chow diet and provided tap water ad libitum. For tissue harvest, mice were sacrificed, and organs were immediately collected and processed for HRR (see below).

Fasting mice studies. These experiments (LANUV AZ: 84-02.04.2017.A102; Figure 3D) were carried out on female C57BL/6J mice aged 15-22 weeks, by removing access to food, but not water, for 16 h.

Heart failure mice studies. For mouse HF studies (LANUV AZ: 81-02.04.2022.A185; Figure 5E-H; Figure S4C), 24-week old male wildtype C57BL/6J mice were purchased from Janvier-Labs. Mice were anesthetized by intraperitoneal (I.P.) injection of ketamine (100 mg/kg; Pfizer Pharma) and xylazine (10 mg/kg; Bayer AG). At this stage, mice underwent permanent left anterior descending artery (LAD) ligation surgery[78]. After intubation of the mice, surgery was conducted under 2 vol% isoflurane anaesthesia as previously described[44]. Ischemic injury was induced via permanent LAD ligation. Typical ST-elevations were used for monitoring and body temperature was controlled continuously. To reduce pain, this open-chest surgery was followed by treatment with buprenorphine (0.1mg/kg, Temgesic®, Indivior) for up to three days. After surgery, mice survived for up to three weeks, inducing chronic HF (left ventricular ejection fraction 28.5± 5.9%), which is an established model of ischemic HF[44]. Age-matched male C57BL/6J mice served as control group. At the end of the experimental protocol, mice were sedated with ketamine and xylazine, as described above. While under aesthesia, blood was collected by cardiac puncture and the left ventricle was excised and processed for HRR (see below). Blood glucose was measured immediately after sacrifice using a glucose meter (StatStrip Xpress, Nova Biomedical GmbH, Mörfelden-Walldorf, Germany).

Kidney cortex DIO mice studies. For these experiments (LANUV AZ: 81-02.04.2021/A218, Figure 7A-C), wildtype C57BL/6J mice aged 10-12 weeks were obtained from Janvier-Labs and were fed a high-fat diet (HFD, Sniff, S7200-E010, 60 kJ % fat) for the duration of 24 weeks to induce obesity. Age-matched controls received normal chow diet (Sniff, V1184-300, 16kJ% fat) for the same duration. Both treatment groups received food and tap water ad libitum. After 24 weeks of HFD or normal chow diet,

mice were sedated with I.P. injection of ketamine (100 mg/kg; Pfizer Pharma) and xylazine (10 mg/kg; Bayer AG). Blood was collected by cardiac puncture and the left kidney was immediately harvested and prepared for HRR, as described below. Blood glucose was measured as described above. Plasma insulin levels were determined with the Ultra Sensitive Mouse Insulin ELISA Kit (90080; Crystal Chem Europe, Zaandam, Netherlands), according to the manufacturer's instructions.

Isolation of primary mouse hepatocytes. Isolation of mouse hepatocytes from 16- to 20-week-old C57BL/6J mice was carried out as previously described[79], with minor modifications. After cervical dislocation, the liver was rapidly exposed and perfused sequentially with EGTA and collagenase solutions through the vena cava at 37˚C. The digested liver was minced gently in suspension buffer and filtered through a 100 µM cell strainer (Corning, Wiesbaden, Germany). Single-cell hepatocytes were separated by low-speed centrifugation at 50 g for 2 min, further purified by Percoll® density gradient (Sigma-Aldrich, Taufkirchen, Germany), and finally suspended in William medium supplemented with 1% penicillin/streptomycin and 10% FBS. Cell viability was assessed by trypan blue dye exclusion. After cell counting, primary hepatocytes were suspended directly in mitochondrial respiration medium (MiRO5; for chemical composition see below) and added to the Oxygraph-2k chambers (Oroboros Instruments, Innsbruck, Austria) at concentration of 50,000 cells/ml.

Human participants and tissue acquisition

The study was performed in accordance with the Declaration of Helsinki and informed consent was acquired upon inclusion to the study from all participants.

Human liver studies. Human liver was obtained from the BARIA_DDZ cohort study (ClinTrials.gov identifier: NCT01477957). All participants provided prior written consent to the study protocol after being informed of the study procedures and risks. The BARIA_DDZ cohort study protocol was approved by the institutional ethics boards of Heinrich-Heine-University Düsseldorf (Germany) and of the North Rhine Medical Association (Germany) (no. 2022-2021_1/no. 2017222). Liver biopsies were obtained by an experienced surgeon approximately 30 min after induction of anesthesia prior to bariatric surgery according to a standardized procedure[34]. Approximately 25 mg of fresh liver tissue were immediately transferred into ice-cooled preservation medium (BIOPS) for HRR; the remaining tissue was immediately snap-frozen in liquid nitrogen and stored at -80°C for further analyses.

Human heart failure studies. Human cardiac ventricle tissue was acquired during cardiac surgery from end-stage HF participants undergoing left ventricular assist device (LVAD) surgery or orthotopic heart transplantation (HTX), from participants with non-ischemic HF undergoing endomyocardial biopsy for diagnostic reasons, as well as from healthy donor hearts of participants after heart transplantation without HF undergoing routine endomyocardial biopsy. LVAD tissue was used for titration protocols to

generate the HBA and ACA Km of human myocardium (Figure 2E, H, M, and P). For comparisons of KB metabolism in HF versus control participants, the HF group was comprised of participants undergoing HTX and participants with non-ischemic HF undergoing endomyocardial biopsy, whereas the control group was comprised of participants after HTX without HF symptoms[42,80]. All HF participants had HF with reduced ejection fraction, whereas all participants in the control group had a preserved left ventricular ejection fraction of above 50% as confirmed via echocardiography and/or cardiac magnetic resonance imaging. Cardiac tissue handling was carried out according to a previously published protocol[42]. All cardiac tissues were stored on ice cooled BIOPS preservation medium immediately after extraction until further processing. Study-related procedures have been approved by the local ethics committee at Heinrich Heine University under the study numbers 5263R, 2021-1635, and 2022-1962 (ClinicalTrials.gov Identifier: NCT05958706).

Human T2D skeletal muscle studies. Human skeletal muscle was acquired from participants in the German Diabetes Study (GDS)[81]. Briefly, GDS is a prospective observational clinical study that enrolls individuals aged 18-69 years diagnosed with type 2 diabetes within the last 12 months based on the criteria of the American Diabetes Association. Exclusion criteria of the GDS compromise diabetes due to other causes, pregnancy, acute or severe chronic heart, renal, liver and psychiatric disease and intake of immunosuppressive therapy. In addition, vastus lateralis skeletal muscle was collected also from healthy volunteers with no first-degree relatives with diabetes, who underwent a 75-g oral glucose tolerance test (AccuCheck Dextro O.G-T., Roche, Basel, Switzerland) to confirm normal glucose tolerance. Insulin sensitivity was assessed during a mixed meal tolerance test (MMTT) using standardized liquid meals (Boost® Nestlé Health Care Nutrition, Lausanne, Switzerland) from the oral glucose insulin sensitivity (OGIS) index, as previously described and validated[52]. Biopsies of skeletal muscle were performed in the region above the vastus lateralis muscle, after the tissue was anaesthetized by subcutaneous injection of 2% lidocaine. Approximately 50-100 mg of tissue was obtained using a modified Bergström needle with suction and immediately stored on ice using BIOPS preservation medium. The GDS was approved by the local ethics committee of the Medical Faculty of the Heinrich Heine University of Düsseldorf (reference number 4508) and is registered at Clinicaltrials.gov (NCT01055093).

HepG2 cells. The human hepatocyte carcinoma cell line HepG2 (American Type Culture Collection, Manassas, Virginia, USA) was cultured at 37°C and 5% CO2 in Dulbecco's Modified Eagle Medium (DMEM) supplemented with 10% FBS (Sigma-Aldrich, Taufkirchen, Germany) and 1% penicillin/streptomycin (ThermoFisher Scientific, Grand Island, USA). Cells were harvested using 0.05% trypsin (PromoCell GmbH, Heidelberg, Germany) when reaching 70–80% confluency and resuspended

in MiRO5. Cell count and viability staining was subsequently performed using acridine orange and propidium iodide and an automated cell counter (DeNovix, Wilmington, USA).

Sample preparation for high-resolution respirometry

Heart, skeletal muscle, and liver tissues were collected in ice-cooled BIOPS (containing [in mM]: 2.77 CaK_2EGTA, 7.23 K_2EGTA, 20 imidazole, 20 taurine, 50 4-morpholine-ethanesulfonic acid, 0.5 dithiothreitol, 6.56 $MgCl_2 \cdot 6H2O$, 5.77 Na_2ATP, and 15 disodium phosphocreatine, pH 7.1), whereas kidney cortex and brain cortex were collected in ice-cooled MiR05 (containing [in mM unless specified]: 0.5 EGTA, 3 MgCl2, 60 K-lactobionate, 20 taurine, 10 KH_2PO_4, 20 HEPES, 110 sucrose and 1 g/L BSA essentially fatty acid-free, pH 7.1) for immediate preparation for HRR[73,82-86].

Sample preparation for HRR was carried out according to standard protocols. In short, fresh cardiac[73] and skeletal muscle fibers[84], were mechanically separated using forceps in ice-cold BIOPS; fresh brain cortex[85] and kidney cortex[86] were cut into small pieces and gently tapped with forceps in ice-cold MiRO5; fresh liver was simply cut in ~2 x 2 mm pieces using forceps in ice-cold BIOPS[82,83], under a light microscope. Subsequently, samples were chemically permeabilized by gentle agitation for 20 min at 4 °C with saponin dissolved in BIOPS (myocardium and skeletal muscle) or MiRO5 (brain cortex and kidney cortex) at a concentration of 50 µg/mL, except for kidney cortex for which 100 µg/mL of saponin were used[86]. For both human and mouse myocardium samples, the saponin step lasted 30 minutes[73]. For the liver, chemical permeabilization was not performed, as previously shown[82,83]. For all tissues, this was followed by three 5-min (or two 10-min for myocardium samples) washing steps in ice cold MiRO5. Cells (primary hepatocytes and HepG2) were added directly to the chambers and following an initial stabilization were permeabilized with 50 µg/million cells of digitonin in the presence of malate and ADP[87].

High-resolution respirometry

Mitochondrial respiration was measured in duplicates (except for Km determinations) in MiR05 at 37 °C, 750 rpm stirrer speed and a chamber volume of 2.0 mL using the high-resolution Oxygraph-2k (Oroboros Instruments, Innsbruck, Austria). For all tissues, oxygen concentration was maintained, via direct syringe injection of pure O_2, between 270 and 480 nmol mL^{-1} for the duration of the experiment, to avoid potential oxygen diffusion limitation[88]. Cytochrome *c* (10 µM) was added to assess the integrity of the outer mitochondrial membrane[89]; samples with a >15% increase post-cytochrome *c* addition were discarded[90]. Mitochondrial respiration in cells was instead assessed at sub-atmospheric oxygen pressure (40 and ~195 nmol ml^{-1}).

HBA dose response for determination of the HBA Km. First, addition of saturating levels of ADP (5 mM) and stabilization of respiration were performed. Waiting times ranging from 10 to 60 minutes

(depending on tissues) were required to reliably measure the small increases induced by the lowest HBA titrations, without the confounding effect of the decrease in JO_2 stemming from exhaustion of endogenous substrates. Subsequently, sodium DL-β-hydroxybutyrate (HBA; racemic mixture of D and L isoforms) was titrated stepwise from 0.01 mM up to 20 mM (mouse heart, kidney cortex, and liver), 30 mM (human heart), 40 mM (mouse soleus and brain cortex, human liver), or 60 mM (human vastus lateralis).

ACA dose response for determination of the ACA Km. First, addition of saturating levels of ADP (5 mM) and malate (2 mM) and stabilization of respiration (for the same reasons above) were performed. ACA was subsequently titrated stepwise from 0.005 mM to 15 mM for all tissues analyzed, with the exception of human heart (up to 30 mM).

Combined ketone body SUIT protocols. To determine the initial step of ketolysis ($[BDH1]_P$; Figure 1, yellow shaded area), which is carried out by BDH1 and does not require the contribution of the TCA cycle, saturating ADP concentrations (5 mM) were first added, followed by brief stabilization and subsequent injection of a single dose of HBA, which was pre-determined via use of an HBA-titration protocol. For ketolysis to proceed (i.e., complete conversion of HBA to acetyl-CoA, which can subsequently enter the TCA cycle and feed reducing equivalents to the ETS), sufficient supply of succinyl-CoA to SCOT is required. This was achieved by addition of the TCA cycle metabolite malate (2 mM). Because these steps encompass complete ketolysis, we named this respiratory state "$[KL]_P$" (Figure 1; green shaded area). It is important to notice that addition of malate as a single substrate has negligible impact on OXPHOS[91]. To gain further insight into the interplay of the various enzymes involved in ketolysis, we included a third step, whereby ACA can be titrated stepwise or added in a single injection. We named this readout "$[KL+ACA]_P$" (Figure 1; blue shaded area). The difference between $[KL+ACA]_P$ and $[KL]_P$ (Δ $[KL+ACA]_P$ - $[KL]_P$) allows to determine whether and to which extent the activity of specific ketolytic enzymes may be rate limiting. In this regard, an increase in JO_2 indicates that addition of ACA provides further substrate for the reaction catalyzed by SCOT/mThiolase, suggesting BDH1 would be rate limiting. A decrease in JO_2 following ACA addition suggests a product-induced inhibition of the equilibrium of the reaction catalyzed by BDH1 (Le Chatelier's principle), since its product (ACA) is now provided at greater concentrations; this would indicate that SCOT/mThiolase do not possess a "reserve capacity" compared to that of BDH1 to further drive ketolysis. OXPHOS capacity was further maximized stimulating convergent electron input through CI by addition of 5 mM pyruvate (except human and mouse myocardium) and 10 mM glutamate ($[KL+ACA+N]_P$), as well as CII, by addition of 10 mM succinate ($[KL+ACA+NS]_P$); the latter respiratory state was used to determine the ratios displayed in Figure 4B and those in Figure 7. Leak (L) respiration, a respiratory state where oxygen consumption is compensating for the back-flux of protons across the mitochondrial membrane,

was subsequently assessed by addition of the ATP-synthase inhibitor oligomycin (2.5 µM; $[KL+ACA+NS]_L$). Maximal uncoupled respiratory ETS (E) capacity ($[KL+ACA+NS]_E$) was assessed by stepwise titration with the protonophore FCCP (0.75-1.5 µM) until maximal respiration was reached. The CIII inhibitor antimycin A (5 µM) was finally added to determine non-mitochondrial oxygen consumption (ROX). A detailed description of the combined KB SUIT protocol for all tissues is presented in Table S6 and S7 for mouse and human organs, respectively). It is important to underline that some of the parameters presented and primarily the various substrates concentrations are species- and pathophysiological state-dependent. Therefore, in future studies, well-designed pilot experiments should be performed to identify the specific parameters and substrate concentrations suitable for each project.

The SUIT protocol utilized to generate Figure S1 was identical to the combined KB SUIT protocol up to addition of HBA, after which 2.5 µM oligomycin were added to stimulate L respiration with electron input through CI via BDH1. Maximal E was subsequently assessed by stepwise titration of FCCP. Addition of 0.5 µM rotenone, an inhibitor of CI, was used to confirm that HBA-linked respiration enters the ETS via CI, as expected (Figure 1). Finally, the CIII inhibitor antimycin A (5 µM) was added to determine non-mitochondrial oxygen consumption (ROX).

NS and FNS SUIT protocols. For determination of the NS or FNS protocols used to calculate the ratios of KB-linked respiration to maximal OXPHOS capacity, and to generate Figure S4, the same concentration of the substrates pyruvate, glutamate, and succinate (as well as 0.2 mM octanoylcarnitine, specific to the FNS pathway protocol) were added in the presence of saturating ADP (5 mM). Substrates of the F pathway were only added in the heart due to its higher physiological reliance on fatty acids[75,76]. Of note, when substrates of the F, N, and S pathways were added after KB substrates, the resulting JO_2 values were lower than in similar protocols without prior addition of KB (Figure S4). The underlying reasons are uncertain, but this underestimation may relate to the utilization of NADH after addition of excess ACA, as this would effectively compete and subtract NADH from entering CI of the ETS. Thus, OXPHOS capacity determined from KB+FNS protocols should not be used interchangeably with OXPHOS capacity assessed from FNS protocols to ensure the internal validity of the ratios determining the relative KB contribution to maximal OXPHOS capacity. Regardless, using a combined protocol (KB+FNS) to determine maximal OXPHOS capacity remains a valuable approach when tissue or machine availability is limited.

Statistical Analysis

Statistical analyses were performed using GraphPad Prism version 10.0.1 (GraphPad Software, San Diego, California, USA) or R version 4.3.0 (R Foundation for Statistical Computing, Vienna, Austria). All values in figures are reported as mean ± SEM. In tables showing cohort characteristics, data are

presented as median with the interquartile ranges or as total number and proportion. Standard distribution was assessed using Shapiro-Wilk tests and visually using normal QQ plots and histograms. Michaelis-Menten kinetics were calculated using GraphPad Prism by subtracting values of mitochondrial respiration prior to first titration of the respective substrate (HBA or ACA) from all values. For comparison of different respiratory states within a single protocol (e.g., Fig. 5 A, B), repeated measurement mixed-effects models (REML) were used with post-hoc pairwise between-group tests. Post-hoc tests were corrected for multiple testing based on the false discovery rate[53]. Simple comparisons between groups without repeated measurements were carried out using paired or unpaired, parametric, or non-parametric tests as specified in the respective figure legends and table footnotes, and according to the underlying study cohort and distribution, respectively. Univariate linear regression models were used to assess the associations of insulin sensitivity and KB respiratory states in human skeletal muscle. An alpha level of 0.05 was considered statistically significant.

References

1. Puchalska, P., and Crawford, P.A. (2017). Multi-dimensional Roles of Ketone Bodies in Fuel Metabolism, Signaling, and Therapeutics. Cell Metab *25*, 262-284. 10.1016/j.cmet.2016.12.022.
2. Fukao, T., Song, X.Q., Mitchell, G.A., Yamaguchi, S., Sukegawa, K., Orii, T., and Kondo, N. (1997). Enzymes of ketone body utilization in human tissues: protein and messenger RNA levels of succinyl-coenzyme A (CoA):3-ketoacid CoA transferase and mitochondrial and cytosolic acetoacetyl-CoA thiolases. Pediatr Res *42*, 498-502. 10.1203/00006450-199710000-00013.
3. Jamshed, H., Beyl, R.A., Della Manna, D.L., Yang, E.S., Ravussin, E., and Peterson, C.M. (2019). Early Time-Restricted Feeding Improves 24-Hour Glucose Levels and Affects Markers of the Circadian Clock, Aging, and Autophagy in Humans. Nutrients *11*. 10.3390/nu11061234.
4. Robinson, A.M., and Williamson, D.H. (1980). Physiological roles of ketone bodies as substrates and signals in mammalian tissues. Physiol Rev *60*, 143-187. 10.1152/physrev.1980.60.1.143.
5. Forbes, J.M., and Thorburn, D.R. (2018). Mitochondrial dysfunction in diabetic kidney disease. Nat Rev Nephrol *14*, 291-312. 10.1038/nrneph.2018.9.
6. Aubert, G., Martin, O.J., Horton, J.L., Lai, L., Vega, R.B., Leone, T.C., Koves, T., Gardell, S.J., Kruger, M., Hoppel, C.L., et al. (2016). The Failing Heart Relies on Ketone Bodies as a Fuel. Circulation *133*, 698-705. 10.1161/CIRCULATIONAHA.115.017355.
7. Yurista, S.R., Chong, C.R., Badimon, J.J., Kelly, D.P., de Boer, R.A., and Westenbrink, B.D. (2021). Therapeutic Potential of Ketone Bodies for Patients With Cardiovascular Disease: JACC State-of-the-Art Review. J Am Coll Cardiol *77*, 1660-1669. 10.1016/j.jacc.2020.12.065.
8. Santos-Gallego, C.G., Requena-Ibanez, J.A., Picatoste, B., Fardman, B., Ishikawa, K., Mazurek, R., Pieper, M., Sartori, S., Rodriguez-Capitan, J., Fuster, V., and Badimon, J.J. (2023). Cardioprotective Effect of Empagliflozin and Circulating Ketone Bodies During Acute Myocardial Infarction. Circ Cardiovasc Imaging *16*, e015298. 10.1161/CIRCIMAGING.123.015298.
9. Berg-Hansen, K., Christensen, K.H., Gopalasingam, N., Nielsen, R., Eiskjaer, H., Moller, N., Birkelund, T., Christensen, S., and Wiggers, H. (2023). Beneficial Effects of Ketone Ester in Patients With Cardiogenic Shock: A Randomized, Controlled, Double-Blind Trial. JACC Heart Fail *11*, 1337-1347. 10.1016/j.jchf.2023.05.029.
10. Garcia-Rodriguez, D., and Gimenez-Cassina, A. (2021). Ketone Bodies in the Brain Beyond Fuel Metabolism: From Excitability to Gene Expression and Cell Signaling. Front Mol Neurosci *14*, 732120. 10.3389/fnmol.2021.732120.
11. Tomita, I., Kume, S., Sugahara, S., Osawa, N., Yamahara, K., Yasuda-Yamahara, M., Takeda, N., Chin-Kanasaki, M., Kaneko, T., Mayoux, E., et al. (2020). SGLT2 Inhibition Mediates Protection from Diabetic Kidney Disease by Promoting Ketone Body-Induced mTORC1 Inhibition. Cell Metab *32*, 404-419 e406. 10.1016/j.cmet.2020.06.020.
12. Rojas-Morales, P., Pedraza-Chaverri, J., and Tapia, E. (2021). Ketone bodies for kidney injury and disease. Advances in Redox Research *2*. 10.1016/j.arres.2021.100009.
13. Mardinoglu, A., Wu, H., Bjornson, E., Zhang, C., Hakkarainen, A., Rasanen, S.M., Lee, S., Mancina, R.M., Bergentall, M., Pietilainen, K.H., et al. (2018). An Integrated Understanding of the Rapid Metabolic Benefits of a Carbohydrate-Restricted Diet on Hepatic Steatosis in Humans. Cell Metab *27*, 559-571 e555. 10.1016/j.cmet.2018.01.005.
14. Koutnik, A.P., Poff, A.M., Ward, N.P., DeBlasi, J.M., Soliven, M.A., Romero, M.A., Roberson, P.A., Fox, C.D., Roberts, M.D., and D'Agostino, D.P. (2020). Ketone Bodies Attenuate Wasting in Models of Atrophy. J Cachexia Sarcopenia Muscle *11*, 973-996. 10.1002/jcsm.12554.
15. Lien, E.C., Westermark, A.M., Zhang, Y., Yuan, C., Li, Z., Lau, A.N., Sapp, K.M., Wolpin, B.M., and Vander Heiden, M.G. (2021). Low glycaemic diets alter lipid metabolism to influence tumour growth. Nature *599*, 302-307. 10.1038/s41586-021-04049-2.
16. Newman, J.C., and Verdin, E. (2014). Ketone bodies as signaling metabolites. Trends Endocrinol Metab *25*, 42-52. 10.1016/j.tem.2013.09.002.

17. Shimazu, T., Hirschey, M.D., Newman, J., He, W., Shirakawa, K., Le Moan, N., Grueter, C.A., Lim, H., Saunders, L.R., Stevens, R.D., et al. (2013). Suppression of oxidative stress by beta-hydroxybutyrate, an endogenous histone deacetylase inhibitor. Science *339*, 211-214. 10.1126/science.1227166.
18. Luukkonen, P.K., Dufour, S., Lyu, K., Zhang, X.M., Hakkarainen, A., Lehtimaki, T.E., Cline, G.W., Petersen, K.F., Shulman, G.I., and Yki-Jarvinen, H. (2020). Effect of a ketogenic diet on hepatic steatosis and hepatic mitochondrial metabolism in nonalcoholic fatty liver disease. Proc Natl Acad Sci U S A *117*, 7347-7354. 10.1073/pnas.1922344117.
19. Cox, P.J., Kirk, T., Ashmore, T., Willerton, K., Evans, R., Smith, A., Murray, A.J., Stubbs, B., West, J., McLure, S.W., et al. (2016). Nutritional Ketosis Alters Fuel Preference and Thereby Endurance Performance in Athletes. Cell Metab *24*, 256-268. 10.1016/j.cmet.2016.07.010.
20. Huang, D., Li, T., Wang, L., Zhang, L., Yan, R., Li, K., Xing, S., Wu, G., Hu, L., Jia, W., et al. (2016). Hepatocellular carcinoma redirects to ketolysis for progression under nutrition deprivation stress. Cell Res *26*, 1112-1130. 10.1038/cr.2016.109.
21. Abdurrachim, D., Teo, X.Q., Woo, C.C., Chan, W.X., Lalic, J., Lam, C.S.P., and Lee, P.T.H. (2019). Empagliflozin reduces myocardial ketone utilization while preserving glucose utilization in diabetic hypertensive heart disease: A hyperpolarized (13) C magnetic resonance spectroscopy study. Diabetes Obes Metab *21*, 357-365. 10.1111/dom.13536.
22. Santos-Gallego, C.G., Requena-Ibanez, J.A., San Antonio, R., Ishikawa, K., Watanabe, S., Picatoste, B., Flores, E., Garcia-Ropero, A., Sanz, J., Hajjar, R.J., et al. (2019). Empagliflozin Ameliorates Adverse Left Ventricular Remodeling in Nondiabetic Heart Failure by Enhancing Myocardial Energetics. J Am Coll Cardiol *73*, 1931-1944. 10.1016/j.jacc.2019.01.056.
23. Pesta, D., and Gnaiger, E. (2012). High-resolution respirometry: OXPHOS protocols for human cells and permeabilized fibers from small biopsies of human muscle. Methods Mol Biol *810*, 25-58. 10.1007/978-1-61779-382-0_3.
24. Granata, C., Jamnick, N.A., and Bishop, D.J. (2018). Training-Induced Changes in Mitochondrial Content and Respiratory Function in Human Skeletal Muscle. Sports Med *48*, 1809-1828. 10.1007/s40279-018-0936-y.
25. Petrick, H.L., Brunetta, H.S., Pignanelli, C., Nunes, E.A., Loon, L.J.C., Burr, J.F., and Holloway, G.P. (2020). In vitro ketone-supported mitochondrial respiration is minimal when other substrates are readily available in cardiac and skeletal muscle. The Journal of Physiology *598*, 4869-4885. 10.1113/jp280032.
26. Georgiev, A., Granata, C., and Roden, M. (2022). The role of mitochondria in the pathophysiology and treatment of common metabolic diseases in humans. Am J Physiol Cell Physiol *322*, C1248-C1259. 10.1152/ajpcell.00035.2022.
27. Rinella, M.E., Lazarus, J.V., Ratziu, V., Francque, S.M., Sanyal, A.J., Kanwal, F., Romero, D., Abdelmalek, M.F., Anstee, Q.M., Arab, J.P., et al. (2023). A multisociety Delphi consensus statement on new fatty liver disease nomenclature. Hepatology *78*, 1966-1986. 10.1097/HEP.0000000000000520.
28. Laffel, L. (1999). Ketone bodies: a review of physiology, pathophysiology and application of monitoring to diabetes. Diabetes/Metabolism Research and Reviews *15*, 412-426. 10.1002/(sici)1520-7560(199911/12)15:6<412::Aid-dmrr72>3.0.Co;2-8.
29. Mannisto, V.T., Simonen, M., Hyysalo, J., Soininen, P., Kangas, A.J., Kaminska, D., Matte, A.K., Venesmaa, S., Kakela, P., Karja, V., et al. (2015). Ketone body production is differentially altered in steatosis and non-alcoholic steatohepatitis in obese humans. Liver Int *35*, 1853-1861. 10.1111/liv.12769.
30. Vijay, N., and Morris, M.E. (2014). Role of monocarboxylate transporters in drug delivery to the brain. Curr Pharm Des *20*, 1487-1498. 10.2174/13816128113199990462.
31. Puchalska, P., Martin, S.E., Huang, X., Lengfeld, J.E., Daniel, B., Graham, M.J., Han, X., Nagy, L., Patti, G.J., and Crawford, P.A. (2019). Hepatocyte-Macrophage Acetoacetate Shuttle Protects against Tissue Fibrosis. Cell Metab *29*, 383-398 e387. 10.1016/j.cmet.2018.10.015.

32. Williams, A.S., Crown, S.B., Lyons, S.P., Koves, T.R., Wilson, R.J., Johnson, J.M., Slentz, D.H., Kelly, D.P., Grimsrud, P.A., Zhang, G.F., and Muoio, D.M. (2024). Ketone flux through BDH1 supports metabolic remodeling of skeletal and cardiac muscles in response to intermittent time-restricted feeding. Cell Metab *36*, 422-437 e428. 10.1016/j.cmet.2024.01.007.
33. Garza-Gonzalez, S., Nieblas, B., Solbes-Gochicoa, M.M., Altamirano, J., and Garcia, N. (2022). Intermittent Fasting as Possible Treatment for Heart Failure. Curr Vasc Pharmacol *20*, 260-271. 10.2174/1570161120666220610151915.
34. Koliaki, C., Szendroedi, J., Kaul, K., Jelenik, T., Nowotny, P., Jankowiak, F., Herder, C., Carstensen, M., Krausch, M., Knoefel, W.T., et al. (2015). Adaptation of hepatic mitochondrial function in humans with non-alcoholic fatty liver is lost in steatohepatitis. Cell Metab *21*, 739-746. 10.1016/j.cmet.2015.04.004.
35. Williamson, D.H., Bates, M.W., Page, M.A., and Krebs, H.A. (1971). Activities of enzymes involved in acetoacetate utilization in adult mammalian tissues. Biochem J *121*, 41-47. 10.1042/bj1210041.
36. Cuenoud, B., Hartweg, M., Godin, J.-P., Croteau, E., Maltais, M., Castellano, C.-A., Carpentier, A.C., and Cunnane, S.C. (2020). Metabolism of Exogenous D-Beta-Hydroxybutyrate, an Energy Substrate Avidly Consumed by the Heart and Kidney. Frontiers in Nutrition *7*. 10.3389/fnut.2020.00013.
37. Ruderman, N.B., Ross, P.S., Berger, M., and Goodman, M.N. (1974). Regulation of glucose and ketone-body metabolism in brain of anaesthetized rats. Biochem J *138*, 1-10. 10.1042/bj1380001.
38. Jedlicka, J., Tuma, Z., Razak, K., Kunc, R., Kala, A., Proskauer Pena, S., Lerchner, T., Jezek, K., and Kuncova, J. (2022). Impact of aging on mitochondrial respiration in various organs. Physiol Res *71*, S227-S236. 10.33549/physiolres.934995.
39. Jensen, N.J., Wodschow, H.Z., Nilsson, M., and Rungby, J. (2020). Effects of Ketone Bodies on Brain Metabolism and Function in Neurodegenerative Diseases. International journal of molecular sciences *21*, 8767. 10.3390/ijms21228767.
40. Owen, O.E., and Reichard, G.A. (1971). Human forearm metabolism during progressive starvation. The Journal of clinical investigation *50 7*, 1536-1545.
41. Barton, R.N. (1973). The interconversion and disposal of ketone bodies in untreated and injured post-absorptive rats. Biochem J *136*, 531-543. 10.1042/bj1360531.
42. Scheiber, D., Jelenik, T., Zweck, E., Horn, P., Schultheiss, H.P., Lassner, D., Boeken, U., Saeed, D., Kelm, M., Roden, M., et al. (2019). High-resolution respirometry in human endomyocardial biopsies shows reduced ventricular oxidative capacity related to heart failure. Exp Mol Med *51*, 16. 10.1038/s12276-019-0214-6.
43. Lemieux, H., Semsroth, S., Antretter, H., Hofer, D., and Gnaiger, E. (2011). Mitochondrial respiratory control and early defects of oxidative phosphorylation in the failing human heart. Int J Biochem Cell Biol *43*, 1729-1738. 10.1016/j.biocel.2011.08.008.
44. Polzin, A., Dannenberg, L., Benkhoff, M., Barcik, M., Keul, P., Ayhan, A., Weske, S., Ahlbrecht, S., Trojovsky, K., Helten, C., et al. (2023). Sphingosine-1-phosphate improves outcome of no-reflow acute myocardial infarction via sphingosine-1-phosphate receptor 1. ESC Heart Fail *10*, 334-341. 10.1002/ehf2.14176.
45. Szendroedi, J., Phielix, E., and Roden, M. (2011). The role of mitochondria in insulin resistance and type 2 diabetes mellitus. Nat Rev Endocrinol *8*, 92-103. 10.1038/nrendo.2011.138.
46. American Diabetes Association (2021). 2. Classification and Diagnosis of Diabetes: Standards of Medical Care in Diabetes-2021. Diabetes Care *44*, S15-S33. 10.2337/dc21-S002.
47. Boushel, R., Gnaiger, E., Schjerling, P., Skovbro, M., Kraunsoe, R., and Dela, F. (2007). Patients with type 2 diabetes have normal mitochondrial function in skeletal muscle. Diabetologia *50*, 790-796. 10.1007/s00125-007-0594-3.
48. Rabol, R., Larsen, S., Hojberg, P.M., Almdal, T., Boushel, R., Haugaard, S.B., Andersen, J.L., Madsbad, S., and Dela, F. (2010). Regional anatomic differences in skeletal muscle

mitochondrial respiration in type 2 diabetes and obesity. J Clin Endocrinol Metab *95*, 857-863. 10.1210/jc.2009-1844.
49. Phielix, E., Schrauwen-Hinderling, V.B., Mensink, M., Lenaers, E., Meex, R., Hoeks, J., Kooi, M.E., Moonen-Kornips, E., Sels, J.P., Hesselink, M.K., and Schrauwen, P. (2008). Lower intrinsic ADP-stimulated mitochondrial respiration underlies in vivo mitochondrial dysfunction in muscle of male type 2 diabetic patients. Diabetes *57*, 2943-2949. 10.2337/db08-0391.
50. Mogensen, M., Sahlin, K., Fernstrom, M., Glintborg, D., Vind, B.F., Beck-Nielsen, H., and Hojlund, K. (2007). Mitochondrial respiration is decreased in skeletal muscle of patients with type 2 diabetes. Diabetes *56*, 1592-1599. 10.2337/db06-0981.
51. Szendroedi, J., Schmid, A.I., Chmelik, M., Toth, C., Brehm, A., Krssak, M., Nowotny, P., Wolzt, M., Waldhausl, W., and Roden, M. (2007). Muscle mitochondrial ATP synthesis and glucose transport/phosphorylation in type 2 diabetes. PLoS Med *4*, e154. 10.1371/journal.pmed.0040154.
52. Tura, A., Chemello, G., Szendroedi, J., Gobl, C., Faerch, K., Vrbikova, J., Pacini, G., Ferrannini, E., and Roden, M. (2018). Prediction of clamp-derived insulin sensitivity from the oral glucose insulin sensitivity index. Diabetologia *61*, 1135-1141. 10.1007/s00125-018-4568-4.
53. Benjamini, Y., Krieger, A.M., and Yekutieli, D. (2006). Adaptive linear step-up procedures that control the false discovery rate. Biometrika *93*, 491-507. 10.1093/biomet/93.3.491.
54. Hamada, S., Takata, T., Yamada, K., Yamamoto, M., Mae, Y., Iyama, T., Ikeda, S., Kanda, T., Sugihara, T., and Isomoto, H. (2022). Steatosis is involved in the progression of kidney disease in a high-fat-diet-induced non-alcoholic steatohepatitis mouse model. PLoS One *17*, e0265461. 10.1371/journal.pone.0265461.
55. D'Agati, V.D., Chagnac, A., de Vries, A.P., Levi, M., Porrini, E., Herman-Edelstein, M., and Praga, M. (2016). Obesity-related glomerulopathy: clinical and pathologic characteristics and pathogenesis. Nat Rev Nephrol *12*, 453-471. 10.1038/nrneph.2016.75.
56. Kleinert, M., Clemmensen, C., Hofmann, S.M., Moore, M.C., Renner, S., Woods, S.C., Huypens, P., Beckers, J., de Angelis, M.H., Schurmann, A., et al. (2018). Animal models of obesity and diabetes mellitus. Nat Rev Endocrinol *14*, 140-162. 10.1038/nrendo.2017.161.
57. Jiang, T., Wang, Z., Proctor, G., Moskowitz, S., Liebman, S.E., Rogers, T., Lucia, M.S., Li, J., and Levi, M. (2005). Diet-induced obesity in C57BL/6J mice causes increased renal lipid accumulation and glomerulosclerosis via a sterol regulatory element-binding protein-1c-dependent pathway. J Biol Chem *280*, 32317-32325. 10.1074/jbc.M500801200.
58. Deji, N., Kume, S., Araki, S., Soumura, M., Sugimoto, T., Isshiki, K., Chin-Kanasaki, M., Sakaguchi, M., Koya, D., Haneda, M., et al. (2009). Structural and functional changes in the kidneys of high-fat diet-induced obese mice. Am J Physiol Renal Physiol *296*, F118-126. 10.1152/ajprenal.00110.2008.
59. Hyotylainen, T., Jerby, L., Petaja, E.M., Mattila, I., Jantti, S., Auvinen, P., Gastaldelli, A., Yki-Jarvinen, H., Ruppin, E., and Oresic, M. (2016). Genome-scale study reveals reduced metabolic adaptability in patients with non-alcoholic fatty liver disease. Nat Commun *7*, 8994. 10.1038/ncomms9994.
60. Targher, G., Corey, K.E., Byrne, C.D., and Roden, M. (2021). The complex link between NAFLD and type 2 diabetes mellitus - mechanisms and treatments. Nat Rev Gastroenterol Hepatol *18*, 599-612. 10.1038/s41575-021-00448-y.
61. Fromenty, B., and Roden, M. (2023). Mitochondrial alterations in fatty liver diseases. J Hepatol *78*, 415-429. 10.1016/j.jhep.2022.09.020.
62. Bedi, K.C., Jr., Snyder, N.W., Brandimarto, J., Aziz, M., Mesaros, C., Worth, A.J., Wang, L.L., Javaheri, A., Blair, I.A., Margulies, K.B., and Rame, J.E. (2016). Evidence for Intramyocardial Disruption of Lipid Metabolism and Increased Myocardial Ketone Utilization in Advanced Human Heart Failure. Circulation *133*, 706-716. 10.1161/CIRCULATIONAHA.115.017545.
63. Berg-Hansen, K., Gopalasingam, N., Christensen, K.H., Ladefoged, B., Andersen, M.J., Poulsen, S.H., Borlaug, B.A., Nielsen, R., Moller, N., and Wiggers, H. (2024). Cardiovascular Effects of Oral Ketone Ester Treatment in Patients With Heart Failure With Reduced Ejection Fraction: A

Randomized, Controlled, Double-Blind Trial. Circulation. 10.1161/CIRCULATIONAHA.123.067971.
64. Brahma, M.K., Wende, A.R., and McCommis, K.S. (2022). CrossTalk opposing view: Ketone bodies are not an important metabolic fuel for the heart. J Physiol *600*, 1005-1007. 10.1113/JP281005.
65. Karwi, Q.G., and Lopaschuk, G.D. (2022). CrossTalk proposal: Ketone bodies are an important metabolic fuel for the heart. J Physiol *600*, 1001-1004. 10.1113/JP281004.
66. Roden, M., and Shulman, G.I. (2019). The integrative biology of type 2 diabetes. Nature *576*, 51-60. 10.1038/s41586-019-1797-8.
67. Okuda, Y., Kawai, K., Ohmori, H., and Yamashita, K. (1991). Ketone body utilization and its metabolic effect in resting muscles of normal and streptozotocin-diabetic rats. Endocrinol Jpn *38*, 245-251. 10.1507/endocrj1954.38.245.
68. Ikeda, T., Ohtani, I., Fujiyama, K., Hoshino, T., Tanaka, Y., Takeuchi, T., and Mashiba, H. (1991). Uptake of beta-hydroxybutyrate in perfused hindquarter of starved and diabetic rats. Metabolism *40*, 1287-1291. 10.1016/0026-0495(91)90030-z.
69. Granata, C., Thallas-Bonke, V., Caruana, N.J., Huynh, K., Qin, C.X., Laskowski, A., Snelson, M., Anthonisz, J., Jap, E., Ramm, G., et al. (2023). 10.1101/2023.10.26.564228.
70. Czajka, A., Ajaz, S., Gnudi, L., Parsade, C.K., Jones, P., Reid, F., and Malik, A.N. (2015). Altered Mitochondrial Function, Mitochondrial DNA and Reduced Metabolic Flexibility in Patients With Diabetic Nephropathy. EBioMedicine *2*, 499-512. 10.1016/j.ebiom.2015.04.002.
71. Hsu, W.Y., Kuo, C.Y., Fukushima, T., Imai, K., Chen, C.M., Lin, P.Y., and Lee, J.A. (2011). Enantioselective determination of 3-hydroxybutyrate in the tissues of normal and streptozotocin-induced diabetic rats of different ages. J Chromatogr B Analyt Technol Biomed Life Sci *879*, 3331-3336. 10.1016/j.jchromb.2011.07.038.
72. Picard, M., Taivassalo, T., Ritchie, D., Wright, K.J., Thomas, M.M., Romestaing, C., and Hepple, R.T. (2011). Mitochondrial structure and function are disrupted by standard isolation methods. PLoS One *6*, e18317. 10.1371/journal.pone.0018317.
73. Scheiber, D., Zweck, E., Jelenik, T., Horn, P., Albermann, S., Masyuk, M., Boeken, U., Saeed, D., Kelm, M., Roden, M., et al. (2018). Reduced Myocardial Mitochondrial ROS Production in Mechanically Unloaded Hearts. J Cardiovasc Transl Res. 10.1007/s12265-018-9803-3.
74. Sharov, V.G., Todor, A.V., Silverman, N., Goldstein, S., and Sabbah, H.N. (2000). Abnormal mitochondrial respiration in failed human myocardium. J Mol Cell Cardiol *32*, 2361-2367. 10.1006/jmcc.2000.1266.
75. Zweck, E., Scheiber, D., Schultheiss, H.P., Kuss, O., Kelm, M., Roden, M., Westenfeld, R., and Szendroedi, J. (2022). Impaired Myocardial Mitochondrial Respiration in Humans With Prediabetes: A Footprint of Prediabetic Cardiomyopathy. Circulation *146*, 1189-1191. 10.1161/CIRCULATIONAHA.122.058995.
76. Zweck, E., Scheiber, D., Jelenik, T., Bonner, F., Horn, P., Pesta, D., Schultheiss, H.P., Boeken, U., Akhyari, P., Lichtenberg, A., et al. (2021). Exposure to Type 2 Diabetes Provokes Mitochondrial Impairment in Apparently Healthy Human Hearts. Diabetes Care *44*, e82-e84. 10.2337/dc20-2255.
77. Gancheva, S., Kahl, S., Pesta, D., Mastrototaro, L., Dewidar, B., Strassburger, K., Sabah, E., Esposito, I., Weiss, J., Sarabhai, T., et al. (2022). Impaired Hepatic Mitochondrial Capacity in Nonalcoholic Steatohepatitis Associated With Type 2 Diabetes. Diabetes Care *45*, 928-937. 10.2337/dc21-1758.
78. Pilz, P.M., Ward, J.E., Chang, W.T., Kiss, A., Bateh, E., Jha, A., Fisch, S., Podesser, B.K., and Liao, R. (2022). Large and Small Animal Models of Heart Failure With Reduced Ejection Fraction. Circ Res *130*, 1888-1905. 10.1161/CIRCRESAHA.122.320246.
79. Hu, J., Srivastava, K., Wieland, M., Runge, A., Mogler, C., Besemfelder, E., Terhardt, D., Vogel, M.J., Cao, L., Korn, C., et al. (2014). Endothelial cell-derived angiopoietin-2 controls liver regeneration as a spatiotemporal rheostat. Science *343*, 416-419. 10.1126/science.1244880.

80. Zweck, E., Karschnia, M., Scheiber, D., Heidecke, H., Dechend, R., Barthuber, C., Kaufmann, S., Kelm, M., Roden, M., Westenfeld, R., et al. (2023). Receptor autoantibodies: Associations with cardiac markers, histology, and function in human non-ischaemic heart failure. ESC Heart Fail *10*, 1258-1269. 10.1002/ehf2.14293.
81. Szendroedi, J., Saxena, A., Weber, K.S., Strassburger, K., Herder, C., Burkart, V., Nowotny, B., Icks, A., Kuss, O., Ziegler, D., et al. (2016). Cohort profile: the German Diabetes Study (GDS). Cardiovasc Diabetol *15*, 59. 10.1186/s12933-016-0374-9.
82. Dewidar, B., Mastrototaro, L., Englisch, C., Ress, C., Granata, C., Rohbeck, E., Pesta, D., Heilmann, G., Wolkersdorfer, M., Esposito, I., et al. (2023). Alterations of hepatic energy metabolism in murine models of obesity, diabetes and fatty liver diseases. EBioMedicine *94*, 104714. 10.1016/j.ebiom.2023.104714.
83. Lund, M.T., Kristensen, M., Hansen, M., Tveskov, L., Floyd, A.K., Stockel, M., Vainer, B., Poulsen, S.S., Helge, J.W., Prats, C., and Dela, F. (2016). Hepatic mitochondrial oxidative phosphorylation is normal in obese patients with and without type 2 diabetes. J Physiol *594*, 4351-4358. 10.1113/JP272105.
84. Granata, C., Caruana, N.J., Botella, J., Jamnick, N.A., Huynh, K., Kuang, J., Janssen, H.A., Reljic, B., Mellett, N.A., Laskowski, A., et al. (2021). High-intensity training induces non-stoichiometric changes in the mitochondrial proteome of human skeletal muscle without reorganisation of respiratory chain content. Nat Commun *12*, 7056. 10.1038/s41467-021-27153-3.
85. Herbst, E.A., and Holloway, G.P. (2015). Permeabilization of brain tissue in situ enables multiregion analysis of mitochondrial function in a single mouse brain. J Physiol *593*, 787-801. 10.1113/jphysiol.2014.285379.
86. Parajuli, N., Shrum, S., Tobacyk, J., Harb, A., Arthur, J.M., and MacMillan-Crow, L.A. (2017). Renal cold storage followed by transplantation impairs expression of key mitochondrial fission and fusion proteins. PLoS One *12*, e0185542. 10.1371/journal.pone.0185542.
87. Piel, S., Chamkha, I., Dehlin, A.K., Ehinger, J.K., Sjovall, F., Elmer, E., and Hansson, M.J. (2020). Cell-permeable succinate prodrugs rescue mitochondrial respiration in cellular models of acute acetaminophen overdose. PLoS One *15*, e0231173. 10.1371/journal.pone.0231173.
88. Granata, C., Oliveira, R.S., Little, J.P., Renner, K., and Bishop, D.J. (2016). Mitochondrial adaptations to high-volume exercise training are rapidly reversed after a reduction in training volume in human skeletal muscle. FASEB J *30*, 3413-3423. 10.1096/fj.201500100R.
89. Granata, C., Oliveira, R.S., Little, J.P., Renner, K., and Bishop, D.J. (2016). Training intensity modulates changes in PGC-1alpha and p53 protein content and mitochondrial respiration, but not markers of mitochondrial content in human skeletal muscle. FASEB J *30*, 959-970. 10.1096/fj.15-276907.
90. Kuang, J., Saner, N.J., Botella, J., Lee, M.J., Granata, C., Wang, Z., Yan, X., Li, J., Genders, A.J., and Bishop, D.J. (2022). Assessing mitochondrial respiration in permeabilized fibres and biomarkers for mitochondrial content in human skeletal muscle. Acta Physiol (Oxf) *234*, e13772. 10.1111/apha.13772.
91. Gnaiger, E. (2012). Mitochondrial Pathways and Respiratory Control: An Introduction to OXPHOS Analysis ; Mitochondr Physiol Network 17.18 (Oroboros Instruments).